

## Models of Five Absorption Line Systems Along the Line of Sight Toward PG0117+213<sup>1,2</sup>

Joseph R. Masiero<sup>3</sup>, Jane C. Charlton<sup>3</sup>, Jie Ding<sup>3</sup>, Christopher W. Churchill<sup>4,5</sup> and Glenn Kacprzak<sup>4</sup>

### ABSTRACT

We present our investigation into the physical conditions of the gas in five intervening quasar absorption line systems along the line of sight toward the quasar PG 0117 + 213, with redshifts of  $z = 0.57$ ,  $z = 0.72$ ,  $z = 1.04$ ,  $z = 1.32$  and  $z = 1.34$ . Photoionization modeling of *HST*, Keck I, and Palomar data, using the code Cloudy, is employed to derive densities and metallicities of the multiple phases of gas required to fit the absorption profile for each system. We discuss the implications of these models for galaxy evolution, including the interpretation of “CIV deficiency” and damped Lyman alpha absorbers (DLAs), and the relationships between galaxy morphology, galaxy luminosity, and absorption signature.

---

<sup>1</sup>Based in part on observations obtained at the W. M. Keck Observatory, which is operated as a scientific partnership among Caltech, the University of California, and NASA. The Observatory was made possible by the generous financial support of the W. M. Keck Foundation.

<sup>2</sup>Based in part on observations obtained with the NASA/ESA *Hubble Space Telescope*, which is operated by the STScI for the Association of Universities for Research in Astronomy, Inc., under NASA contract NAS 5-26555.

<sup>3</sup>Department of Astronomy and Astrophysics, The Pennsylvania State University, University Park, PA 16802, *masiero, charlton, ding@astro.psu.edu*

<sup>4</sup>Department of Astronomy, New Mexico State University 1320 Frenger Mall, Las Cruces, New Mexico 88003-8001, *cwc, glennk@nmsu.edu*

<sup>5</sup>Visiting Astronomer at the W. M. Keck Observatory

*Subject headings:* quasars: absorption lines — galaxies: evolution — galaxies: halos — intergalactic medium

## 1. Introduction

Quasar absorption line analysis is a powerful tool for studying the properties of different types of gas in the universe, including gas around quasars, disks and halos of intervening galaxies, and high velocity clouds. This paper focuses on the MgII absorption line systems produced by five intervening galaxies along the line of sight toward the quasar PG 0117+213. The most difficult part of analyzing quasar absorption lines is connecting the velocity space absorption profiles that are observed in the quasar’s spectrum with the physical properties of the gas that is creating the profile. In particular, trying to associate intervening absorption systems with particular types of structures in galaxies has proven to be difficult. Two methods for making this association are imaging the field around the quasar and looking for galaxies at the same redshifts as the absorption systems, and indirectly comparing properties determined from the absorption profiles with physical properties and processes that are known to occur in galaxy halos and disks. There are difficulties with each, however. Imaging a galaxy becomes practically impossible for large redshifts, dwarf galaxy hosts, or galaxies at small impact parameters from the quasar. On the other hand, velocity profiles can be very complicated, involving rotation, thermal components, gaseous expulsion, collisions, unresolved features, and unrelated absorption.

The MgII  $\lambda\lambda 2796, 2803$  doublet is a key identification tool for absorption systems, due to its strength, 2 : 1 doublet ratio, and location in the optical for moderate redshifts ( $0.3 < z < 2.4$ ). MgII absorbers can be divided into two different types: weak, with equivalent widths  $< 0.3 \text{ \AA}$ , and strong, with equivalent widths  $\geq 0.3 \text{ \AA}$ . The division of  $0.3 \text{ \AA}$  was historically chosen as an artifact of observational sensitivity (Steidel & Sargent 1992), however it also may have some significance as the approximate transition point in the neutral hydrogen between optically thin and optically thick (Rigby et al. 2002). Weak MgII systems can be further subdivided into two main categories. Single cloud weak absorbers are isolated, narrow clouds with Doppler parameters  $2 < b < 8 \text{ km s}^{-1}$  (Churchill et al. 1999b). Multiple cloud weak absorbers are a collection of single, weak MgII clouds within a narrow, related velocity range (e.g.  $300 \text{ km s}^{-1}$ ) with a total equivalent width of  $< 0.3 \text{ \AA}$ . Typically, strong MgII absorbers are saturated, and weak ones are unsaturated, however there are important exceptions to this generalization. One example of such a case would be a multiple cloud system with a total equivalent width greater than  $0.3 \text{ \AA}$  (and therefore classified as a strong

MgII system), which in actuality is a collection of unsaturated weak MgII clouds. Also, it should be noted that an unresolved weak MgII cloud can be saturated while not being completely black in the core. This is a very important phenomenon to be aware of when modeling very narrow weak MgII clouds, as it can strongly affect the modeling results (Ding et al. 2003a).

Single cloud weak MgII absorbers have properties consistent with small pockets or sheets of low ionization gas associated with highly-ionized extended gas structures, but most are not known to be associated with any intervening galaxy (Rigby et al. 2002). One multiple cloud weak MgII absorber has been hypothesized to be a superwind coming off of one or a pair of dwarf galaxies (Zonak et al. 2004). Others are thought to be collections of weak clouds all belonging to the same host galaxy as extensions of the strong MgII absorber population.

In the past, high resolution coverage of multiple ionic transitions enabled the modeling of physical conditions of quasar absorption line systems at low redshift (Sembach et al. 1995; Tripp, Lu, & Savage 1996, 1997; Sembach et al. 1999; Chen & Prochaska 2000). This paper is not the first to analyze intermediate redshift,  $z \sim 1$ , MgII systems along the line of sight toward a quasar, however few other absorption systems at that redshift have been analyzed to the level of detail we present here. Previous detailed studies that have used the same modeling method include Ding et al. (2003b), who modeled what they believe to be a double galaxy at redshift  $z = 0.93$  along the line of sight toward PG 1206 + 459, which had drastically different high ionization structure for each of the galaxies, and Ding et al. (2003a), who considered an absorption system at  $z = 0.99$  toward PG 1634 + 706 which was deficient in CIV, potentially due to a low metallicity or very high ionization broad HI absorption phase. Several weak MgII absorbers, single and multiple cloud, have been modeled in detail (Charlton et al. 2003; Zonak et al. 2004). We have also recently completed a similar study of six MgII absorption systems along the PG 1241 + 176, PG 1248 + 401, and PG 1317 + 274 lines of sight (Ding et al. 2004). Each new system studied in such detail has added new insights into the mix of processes that determine gas structure formation.

The number of detailed studies at  $z \sim 1$  has been limited because both high resolution and coverage of many different absorption species are required to accurately constrain a model. PG 0117 + 213 is ideal for a study like this because it is bright in both the optical and UV, and it has five intervening MgII absorbers in one high resolution spectrum. These systems were discussed in an earlier paper by Churchill et al. (2000a), however they did not have the benefit of the high resolution UV coverage of many important transitions by the Space Telescope Imaging Spectrograph onboard the *Hubble Space Telescope* (*HST/STIS*).

In this paper, we present photoionization and collisional ionization models of the sub-components of the five intervening MgII systems, also known as clouds, which were made to

determine the physical properties of the gas, such as ionization parameter and metallicity. Our model clouds were ionized by the Haardt-Madau extragalactic background radiation (Haardt & Madau 1996). The values for the ionization parameters of the clouds are used to separate them into distinct regimes called phases. These phases, characterized by the density of the gas, are broadly divided by the different types of ionization they exhibit: high, low, or very-low. Many absorption line systems show multiple phases that overlap in velocity space, but have very distinct kinematic profiles. When many absorption species are available as constraints, applying models with overlapping phases of ionization to these multi-phase systems allows for very detailed models of the absorption lines to be created.

We describe our data and processing techniques in § 2. Next, we describe in depth our method for modeling quasar absorption lines in § 3. We then present our modeling results and a discussion of their significance in § 4. Note that in this section, we discuss each of the five systems in separate subsections. We summarize our results in § 5, and state our conclusions in § 6.

## 2. Data and Processing

### 2.1. The Data

Spectra from the *HST*, the Keck I telescope, and the Palomar 200 inch telescope were used to constrain our models. The Keck I High Resolution Spectrometer (HIRES, Vogt et al. (1994)) spectrum covers a wavelength range of 4317.7 Å to 6775.1 Å, with a resolution of 45000 and a signal-to-noise of around 30 per pixel. This spectrum was reduced in the standard way using IRAF, as described in Churchill et al. (2000a). The *HST*/STIS spectrum was obtained using the E230M grating with a 0.2" slit width, and a central wavelength of 2707 Å. The spectrum covers a wavelength range of 2303 to 3111 Å, with a resolution of 30000. This spectrum was reduced with the standard STIS pipeline (Brown et al. 2002). The overlapping sections of the spectrum were co-added. The combined spectrum has a signal-to-noise range of 4 – 9 per pixel, based on the standard deviation of the data points.

A *HST* Faint Object Spectrograph (FOS) spectrum, obtained with the G190H grating, covers a wavelength range of 1574 Å to 2331 Å, and has a resolution of 1300. This spectrum was reduced as part of the QSO Absorption Line Key Project (Bahcall et al. 1993, 1996; Jannuzi et al. 1998). This spectrum was obtained using the spectropolarimetry mode, with a 1.0" aperture (Koratkar et al. 1998). Only the Ly $\alpha$  line from the  $z = 0.5764$  damped Ly $\alpha$  absorber (DLA) was detected in this relatively noisy spectrum. Because of this, we use it primarily as a constraint on the Lyman limit breaks of our systems. The ground based

spectrum covering the CIV doublet for the  $z = 1.3250$  and  $z = 1.3430$  systems was taken from Steidel & Sargent (1992), who used the Palomar 200 inch telescope. This spectrum has a resolution of 860.

To fit the STIS spectrum, the echelle orders were combined into one large file, and then broken up into a few large regions. The unabsorbed sections of continuum were chosen for each region, and variable order polynomials were fit to the continuum. The spectrum was then normalized with these polynomials in order to facilitate a search for absorption features. The HIRES spectrum was fit with Legendre polynomials as described in Churchill et al. (2000a) (and references therein).

Because the G190H FOS data covered the three Lyman limit breaks almost exclusively, there were very few points that could be considered continuum, and so the continuum was generally assumed to be flat in the region redward of the  $z = 1.3430$  Lyman limit break, and extrapolated over the Lyman limit breaks.

The data from all the instruments that is relevant to constraining each of the five systems is presented in Figures 1-5. Tables 1-5 present the equivalent widths or the  $3\sigma$  equivalent width limits for the displayed transitions.

## 2.2. Galaxy Identification

One potential candidate and one confirmed galaxy were found to be associated with absorption systems seen toward PG 0117 + 213 by Churchill et al. (1996) (and references therein). Both were imaged with broadband filters ( $g(4900/700)$ ,  $R(6930/1500)$ ,  $i(8000/1450)$ , and NICMOS) which allowed for the determination of the rest frame  $B$  and  $K$  magnitudes. The galaxy candidate thought to be associated with the  $z = 0.5764$  absorption system has a  $B$  luminosity of  $2.32L_B^*$  (where  $L_B^*$  is the  $B$ -band Schechter luminosity, and for  $q_0 = 0.05$  and  $h = H_0/100\text{kms}^{-1}\text{Mpc}^{-1} = 1$  as it was tabulated in Churchill et al. (1996)), a  $B-K$  of 4.00, and an impact parameter of  $5.1 h^{-1}$  kpc. This galaxy candidate is too close to the quasar to be able to be classified morphologically, though it has a very red color, meaning it could be an elliptical galaxy or a very red spiral galaxy. The confirmed galaxy at  $z = 0.7290$  has a  $B$  luminosity of  $3.27L_B^*$  (from Churchill et al. (1996), again using  $q_0 = 0.05$  and  $h = 1$ ), a  $B-K$  of 4.02, and an impact parameter of  $36.0 h^{-1}$  kpc. The galaxy at  $z = 0.7290$  is a face on, barred spiral; approximately SBa (Kacprzak et al. 2004).

There are three other galaxies within 10 " of the quasar which are potential candidates for the  $z = 1.0480$ ,  $1.3250$ , and  $1.3430$  absorption systems, all  $\sim 3$  magnitudes fainter than the  $3.27L_B^*$  galaxy associated with the  $z = 0.7290$  absorber (Kacprzak et al. 2004). In

particular, one galaxy candidate, if at  $z = 1.0480$ , would have an impact parameter of  $22.7 h^{-1}$  kpc (using  $q_0 = 0.05$  and  $h = 1$ , as in Churchill et al. (1996), for consistency), making it a likely candidate for the strong absorber.

### 3. Modeling Techniques

Through the use of photoionization and collisional ionization models, we constrain the ionization conditions, metallicities, chemical compositions, and kinematic makeup of five systems along the line of sight toward PG 0117 + 213. These methods are the same as were employed in Charlton et al. (2003), Ding et al. (2003a), Ding et al. (2003b), and Zonak et al. (2004).

For all five systems, we began our modeling by focusing on the absorption features in the Keck I/HIRES data, since they had the highest signal-to-noise and resolution of the spectra available. For all but the primary component of the  $z = 0.5764$  system, we used the MgII  $\lambda\lambda 2796, 2803$  transitions as a “kinematic template”. We found a minimum number of Voigt profile components required to fit the observed structure of the kinematic template transition. For the  $z = 0.5764$  system, we used the MgI 2853 to determine a kinematic template for fitting the primary component, since the MgII profiles were saturated.

For our photoionization models, we used an ionizing background spectrum determined at the redshift of each system, based on the most current Haardt-Madau extragalactic background radiation spectrum available (Haardt & Madau 2001). The spectrum for each redshift was determined by linearly interpolating between the tabulated redshift values. We adopted a model ionizing spectrum that included contributions from star-forming galaxies (with a relatively high escape fraction of 10%) as well as from quasars. The effect of absorption by the intervening Ly $\alpha$  forest clouds was also included. A quasar-only spectrum would be harder and would generally lead to stronger high ionization absorption. We discuss the effects of using such a spectrum in § 3.5.

In general, it was not possible to produce the observed absorption in all ionization stages, and at all velocities, from the original kinematic template. A minimum of one to three phases of gas were required to fit all transitions in a given system. Each phase can be placed into one of four different regimes: low ionization, very-low ionization, high ionization, or a general “Other” category. Clouds are defined as falling in the low ionization regime if the ionization parameter,  $U$ , (defined as the ratio of the number density of ionizing photons to the number density of hydrogen) is in the range  $-5 < \log U < -2.5$ . In this case, the majority of the MgII absorption would arise from low ionization clouds. Clouds in the very-low ionization

regime, with  $\log U < -5$ , generally give rise to significant amounts of absorption from neutral species. High ionization clouds are defined as those with  $\log U > -2.5$ ; they may have detected CIV, NV, and/or OVI absorption, and may, in principle be photoionized or collisionally ionized. The “Other” category consists of clouds that do not fall cleanly into one of these regimes, either because they fall in between regimes, because they are collisionally ionized, or because they cannot be constrained well enough to be classified. The ionization fraction can be defined as the ratio of neutral to total hydrogen and for our models this can be read from Tables 6–10. The ionization fraction is closely related to  $\log U$ , but there can be a dependence on metallicity.

### 3.1. The Low Ionization Phase

Initially, we assumed that all of the observed MgI was made in the same phase as the MgII. We applied photoionization models to these MgII clouds, adjusting the parameters to fit the observed MgI, as well as the other lower-ionization transitions, such as FeII, OI, SiII, and CII, when these transitions were covered. For most of our systems, this method provided adequate models of the observed lower-ionization gas. To constrain a model of a system, we first used a minimum number of Voigt profiles to fit the MgII (or MgI as mentioned above for the  $z = 0.5764$  system) (Churchill & Vogt 2001), giving us a column density and Doppler parameter value for each component. We then used Cloudy, version 94.0 (Ferland 2001), with various values of ionization parameter and metallicity, to find expected column densities for the other observed transitions. The thermal Doppler parameter for each chemical element was determined using the cloud temperature given by Cloudy, and combined with the Doppler parameter due to turbulence/bulk motion to obtain the total model Doppler parameter for that element. The turbulence/bulk motion Doppler parameter was calculated based on the observed Doppler parameter for the kinematic template transition. Synthetic line profiles based on the model column densities and Doppler parameters were convolved with the line-spread functions of the appropriate spectrograph, creating models of the contribution of the low ionization phase to all observed transitions. We adjusted the ionization parameter and metallicity to fit the observed MgII, MgI, and FeII profiles, and the available Ly $\alpha$  and/or Lyman Limit features. In many cases, these models consistently produced the other observed low ionization transitions (e.g. AlII, CII, and SiII).

We found for our “best-fit” models metallicities in the range of  $-2.0 \leq \log \frac{Z}{Z_{\odot}} \leq 1.0$  for the low ionization phase, while ionization parameters were in the range of  $-5.0 \leq \log U \leq -2.0$ . Our criterion for a “best-fit” model was that the model adequately fit the largest number of transitions with the fewest number of components. In some cases, adjustments had to be

made to the abundance patterns for the model to correctly match all the observed transitions. Although we considered a strict  $\chi^2$  statistic, we found that individual pixels (which could be influenced by blends or correlated noise) often dominate this value. A “by-eye” comparison of the models to the data generally produced ionization parameters and metallicities accurate to  $\sim 0.1$  dex. This process was illustrated in Fig. 6 of Rigby et al. (2002). Our “best-fit” models of contributions from the low ionization phase are superimposed (as dashed curves) on the data in Figures 1-5.

In one case (the  $z = 0.5764$  system), this method could not fit all of the observed transitions, calling for the addition of a very-low ionization phase. In three of the systems ( $z = 1.3430$ ,  $z = 1.3250$ , and  $z = 0.5764$ ), higher ionization transitions, such as CIV, NV, and OVI, were also observed, but could not be produced adequately by the low ionization phase clouds (see the dot-dash curves in Figures 1, 2, and 5). This was sometimes due to constraints on the ionization parameter based on very-low and low ionization transitions, and sometimes due to distinct differences between the kinematic structure of the high and low ionization phase profiles. This called for the addition of a high ionization phase in these three cases. In three systems ( $z = 1.0480$ ,  $z = 1.3250$  and  $z = 1.3430$ ), an HI-only cloud was needed to produce all the observed hydrogen absorption. In the first two cases, these HI clouds were far removed in velocity space from the rest of the absorption features.

### 3.2. The Very-Low Ionization Phase

For the primary absorption region of the  $z = 0.5764$  absorber, we were unable to use MgII as a kinematic template to determine ionization parameters consistent with the other very-low and low ionization transitions (for any assumed metallicity). At first, we believed this problem to be a result of ambiguity of the MgII absorption strength, due to saturation. However, after exploring a wide range of Voigt profile fits to the MgII, we were unable to find any model that satisfactorily fit the observed MgII, MgI, CaII and TiII. We were able to reconcile this by adding a very-low ionization phase. The kinematic template for this phase was drawn from a Voigt profile fit to the MgI. Using this template we tried to determine ionization parameters and metallicities that would produce the observed CaII, TiII, and FeII absorption. Over the full range of parameters, TiII and FeII were underproduced, and abundance pattern variations were considered. The addition of a very-low ionization phase and the optimal parameters given in the “best fit” model (Table 10) are consistent with the philosophy of minimizing the required abundance pattern adjustments. The contribution of the very-low ionization phase can be seen as the dotted line in Figure 5. The low ionization phase for  $z = 0.5764$  was then constrained by SiII, MgII, AlII, AlIII.



It is possible that very-low ionization phases would exist in other systems, however they are not necessary to explain absorption in the observed transitions in those cases. If a very-low ionization phase did exist in one of the other systems, the parameters of its low ionization phase would have to be adjusted to compensate.

### 3.3. The High Ionization Phase

After the very-low and low ionization transitions had been modeled, the OVI, NV, and CIV absorption of three systems ( $z = 1.3430$ ,  $z = 1.3250$ , and  $z = 0.5764$ ) was still underproduced. In the case of the  $z = 0.5764$  system, the higher ionization absorption at the same velocity as the low ionization absorption (at  $v = -30$  and  $-9 \text{ km s}^{-1}$ ) could be produced by the low ionization phase. However, for the high ionization absorption observed at other velocities, as well as the absorption in the other two systems, the kinematic profiles of the high ionization absorption were so different from that of the underlying low ionization absorption that they could only be fit by adding a high ionization phase. In the case of the  $z = 0.5764$  system, the high ionization phase was unconstrained, apart from the lack of production of low ionization transitions. For the  $z = 1.3250$  and  $z = 1.3430$  systems, this phase was constrained by CIV, NV, and OVI.

In principle, either photoionization or collisional ionization could determine the ionization balance for the high ionization phase of a given component. We were able to differentiate between systems that required collisional ionization models and those that could be consistent with photoionization models by comparing the different absorption patterns each creates. Collisionally ionized clouds tend to produce a narrow range of ionized transitions (e.g. CIV or NV or OVI, but never all three), whereas photoionized clouds tend to have broader ranges. Our high ionization components are shown in the figures as the dot-dashed line. The significance of the lack of a high ionization phase in the  $z = 1.0480$  and  $z = 0.7290$  systems will be discussed in § 4.3.2 and § 4.4.2.

An illustration of how the parameters of high ionization components are typically constrained by our modeling technique was given in Zonak et al. (2004). Since the high ionization gas is in the optically thin regime, the ionization parameter can be determined from the ratio of any two high ionization transitions, independent of metallicity. The metallicity is then constrained, for that ionization parameter, based upon the  $\text{Ly}\alpha$  and  $\text{Ly}\beta$  transitions, particularly for our  $z = 1.3430$  and  $z = 1.3250$  systems.

### 3.4. Other Phases

Two of our systems,  $z = 1.0480$  and  $z = 1.3250$ , required an additional HI-only cloud to be added to fill out the observed Ly $\alpha$  profile. In both cases, the cloud was added to fill out the blueward wing of the Ly $\alpha$  profile, at  $v = -270 \text{ km s}^{-1}$  for the  $z = 1.0480$  system, and at  $v = -140 \text{ km s}^{-1}$  for the  $z = 1.3250$  system. In order to get a rough idea on how the excess Ly $\alpha$  absorption might be produced, we considered a simple single HI-only cloud model for each absorbers. The metallicities of these clouds were required to be low in order not to produce metal lines at the same velocities.

The  $z = 1.3430$  system also required an additional Ly $\alpha$  component, however this cloud was a broad absorber, covering the full velocity range of the system. It primarily produced the wings of the Ly $\alpha$  profile.

A SiIII component was added to the  $z = 1.0480$  system to fill out the SiIII 1207 and Ly $\alpha$  absorption at  $v \sim -200 \text{ km s}^{-1}$ . This helped produce much of the Ly $\alpha$  absorption in that velocity range, but a HI-only cloud was still required for this system, as discussed above.

Also, a collisionally ionized phase was added into the  $z = 1.0480$  system in order to fit the excess SiIV absorption observed at a position of  $6 \text{ km s}^{-1}$ . Although the SiIV 1394 is blended from  $-300 \leq v \leq 100 \text{ km s}^{-1}$ , the SiIV 1403 matches the main spike of the SiIV 1394 at  $v = 6 \text{ km s}^{-1}$ , giving us reason to believe that at least that small part is a real feature. Our reasons for choosing a collisionally ionized phase, as opposed to a photoionized phase, will be discussed in §4.3.1.

### 3.5. Input Spectra Variations

We used an input spectrum which is an updated version of the spectrum presented in Haardt & Madau (1996). We obtained the new spectrum from Haardt & Madau (2001), which was an extragalactic background radiation spectrum from quasars, similar to the original, but with additional contributions from star forming galaxies with an escape fraction of 10%. We chose to use this spectrum, as opposed to the older one, because our systems exist during an epoch of increased star formation ( $z \approx 1$ ) so that we would expect some stellar contribution. The primary effect of using a QSO-only spectrum is an increase in high ionization absorption contributed by the lower ionization clouds, which is a result of this spectrum being harder than the spectrum with star forming galaxies. As we discuss in § 4, all of our models either produced too much high ionization absorption to begin with, or had the high ionization gas so far offset from the lower ionization gas that making more in the

lower ionization phases would not adequately model the data. A more thorough study of the effects of varying the spectral shape on models of some other absorption systems is presented in Ding et al. (2004).

## 4. Model Results and Discussion

We now present our numerical constraints on the properties of the five MgII systems we analyzed in the line of sight toward PG 0117 + 213. Photoionization modeling was used to determine the range of acceptable ionization parameters ( $\log U$ ) and metallicities ( $\log Z$ ), when adequate constraints were available. Collisional ionization was also considered and temperatures ( $\log T$ ) were constrained for possible collisional models. The transitions used to constrain these values are listed, when appropriate. The sample models were overlaid on the data, and are presented in Figures 1-5. The equivalent widths of key transitions of each system are given in Tables 1-5. The input parameters used to create our models, as well as some of the derived parameters are given in Tables 6-10. The tick marks in the figures indicate the locations of model clouds from the tables, as noted specifically in the figure captions. The redshifts given for each system are optical depth weighted mean values derived from the MgII transitions observed by Keck I/HIRES. Because the Lyman limit break due to the  $z = 1.3430$  system affects the modeling of the  $z = 1.3250$  system, we present results starting with the highest redshift system and ending with the lowest.

### 4.1. The $z = 1.3430$ System

#### 4.1.1. Results

Figure 1 shows key transitions covered in the Keck I/HIRES and *HST*/STIS spectra for this system. The MgII 2803 in the Keck I/HIRES spectrum was fit with a total of five Voigt profile components from  $-137 \text{ km s}^{-1}$  to  $11 \text{ km s}^{-1}$  (Churchill, Vogt, & Charlton 2003), clouds MgII<sub>1</sub>–MgII<sub>5</sub>, given in Table 6. The rest frame equivalent width of MgII 2803 is  $W_r(2803) = 0.147 \pm 0.004 \text{ \AA}$  (Churchill et al. 1999b). MgII 2796 fell off an echelle order, so we do not know its equivalent width, but it is likely that this is a multiple cloud, weak MgII absorber, below the  $W_r(2796) = 0.3 \text{ \AA}$  cutoff for strong systems. The strongest component was blended with a weaker component to the red, giving rise to an asymmetric profile. FeII is detected only in the strongest component (cloud MgII<sub>4</sub> at  $v = 1 \text{ km s}^{-1}$ ). In the STIS spectrum, SiII 1260 and SiII 1190 are detected, but the former is too strong relative to the latter to be consistent with a Voigt profile fit. SiII 1193 cannot be used as a constraint

because it is blended with Galactic MgII 2796. We adopt SiII 1190 as the most adequate constraint on  $N(\text{SiII})$ . CII 1036 is detected in the STIS spectrum. Unfortunately, the stronger transition, CII 1335, is not covered. NII 1084 is affected by a blend with OVI 1038 at  $z = 1.4477$ .

The intermediate ionization transitions for this system are strongly affected by blends. SiIII 1207 is blended with the Ly $\alpha$  line from the  $z = 1.3250$  system, and cannot be studied. A strong line is detected at the expected position of CIII 977. This line seems quite strong relative to the other lines from this system, and could suffer from a blend. However, we could not confirm that the blend is with a Ly $\alpha$  line at  $z = 0.8826$  because CIV 1551 for that system is not detected and Ly $\beta$  is not covered in the spectrum. We will consider both the possibility that all of the absorption is CIII 977 at  $z = 1.3430$  and the possibility that there is a blend affecting it. NIII 989 may also be blended with a Ly $\alpha$  line at  $z = 0.9077$ , but there is nothing to confirm this identification.

The high ionization transitions, NV  $\lambda\lambda 1239, 1243$  and OVI  $\lambda\lambda 1032, 1038$  are detected in the STIS spectrum. Equivalent widths for these transitions are listed in Table 1. The NV 1239 transition is blended with Ly $\alpha$  from a system at  $z = 1.3866$ , but the NV 1243 transition appears to be relatively unaffected by blends. NV is detected in components centered at  $v = -147 \text{ km s}^{-1}$  and  $v = -44 \text{ km s}^{-1}$ , clouds OVI<sub>1</sub> and CIV<sub>1</sub> in Table 6. OVI 1032 is also detected in cloud CIV<sub>1</sub> at  $v = -147 \text{ km s}^{-1}$ , but it is unclear if the detection blueward of  $-100 \text{ km s}^{-1}$  is real or a blend. A blend with Ly $\gamma$  from a  $z = 1.4986$  system is known to affect OVI 1038 in that region. CIV  $\lambda\lambda 1548, 1551$  is detected in a low resolution FOS spectrum. The CIV is strongest at wavelengths corresponding to the blueward component in NV, and not to the strongest low ionization component.

The metallicity of the low ionization phase of this system can be constrained by Ly $\alpha$  and Ly $\beta$  as well as by a partial Lyman limit break observed at the corresponding wavelength in the lower resolution FOS spectrum, also shown in Figure 1. The situation is significantly complicated by the fact that the breaks due to the  $z = 1.3250$  and  $z = 1.3430$  systems are superimposed. To make matters worse, the continuum fit in the region above the partial Lyman limit break is highly uncertain, with different fits giving an optical depth range of  $\tau \approx 1.3 \pm 0.2$ , to one sigma. We derive constraints on the  $z = 1.3430$  system, taking into account the uncertainty in the continuum fit, and assuming that none or all of the break could arise from it. Then we apply these constraints to find a consistent solution for the  $z = 1.3250$  system.

We begin with the five component Voigt profile fit to MgII 2803. FeII 2383 provides a constraint on the ionization parameter of  $-3.9$  to  $-4.0$  for the main component, cloud MgII<sub>4</sub>. The other four low ionization clouds do not have well constrained ionization parameters,

with only weak upper limits provided by NII 989 and CII 1335. We pushed the ionization parameter values for these clouds (MgII<sub>1</sub>–MgII<sub>3</sub> and MgII<sub>5</sub>) as high as possible in order to maximize the production of CIII 977. The contribution of this phase of gas is shown as a dashed line on Figure 1. High ionization transitions are not significantly produced in this phase.

Next we consider metallicity constraints for the MgII clouds. We simplified our models by assuming that all the MgII clouds in this system (MgII<sub>1</sub>–MgII<sub>5</sub>) had the same metallicity. The simplest model of the Lyman limit break would have the  $z = 1.3430$  system produce the full Lyman limit break absorption. This model would also produce most of the Ly $\beta$  absorption in the same clouds. For the Ly $\beta$ , it is possible to fit the width of the saturated trough with the narrow, low ionization clouds, but it is not possible to fit the blue wing. Ly $\alpha$  still requires additional broad components to fit both wings. All five clouds have a metallicity of  $\sim -0.8$  in a model that best fits Ly $\beta$  and the partial Lyman limit break, but the uncertainty is large ( $\pm 0.2$  or  $0.3$  dex) due to the large uncertainty in the continuum fit. However, if we let the  $z = 1.3250$  system have a contribution to the Lyman limit break that is comparable to the  $z = 1.3430$  system, we find a metallicity value of  $\sim -0.3$  for both systems, with the same uncertainty of  $\pm 0.2$  or  $0.3$  dex. An additional Ly $\alpha$  component is still required for the  $z = 1.3430$  system in this case, but the model fits the Lyman limit break more consistently in the latter case, and so we use this case for the model displayed in Figure 1, as well as the numbers given in Table 6. This finding supports the predictions of Churchill et al. (2000a), who found that the metallicities of these two systems should be equal, through modeling of a lower resolution spectrum of the Lyman limit break.

The contributions of this  $\log Z = -0.3$  model, for the low ionization clouds, to Ly $\alpha$ , Ly $\beta$ , and the partial Lyman limit break are shown in Figure 1. Since we have assumed the same metallicity for the five low ionization clouds, among the five, the main component at  $1 \text{ km s}^{-1}$  is the dominant contributor to the Lyman limit break.

In order to fill in the Ly $\alpha$  profile, an additional broad Ly $\alpha$  component, Ly $\alpha_1$  in Table 6, is required. This cloud was placed roughly at the center of the main Ly $\alpha$  absorption ( $z \simeq -73 \text{ km s}^{-1}$ ), and is constrained to have low metallicity ( $\log Z < -2.5$ ) so as not to produce metal transitions. In order to correctly produce the observed absorption wings, a minimum Doppler parameter of  $b \approx 45 \text{ km s}^{-1}$  is required, which leads to a minimum column density of  $\log N = 16.6 \text{ cm}^{-2}$  (we adopted  $\log N = 16.8 \text{ cm}^{-2}$  in Table 6 and Figure 1, since this model provides a slightly better fit to the Ly $\alpha$  profile). This column density is larger than  $N(\text{HI})$  for the low ionization clouds, so that this broad Ly $\alpha$  component dominates the Lyman limit break for this system.

The high ionization transitions (CIV, NV, and OVI) cannot be produced by the MgII

clouds. They do not occur at the same velocities as the strong, low ionization absorption. The redward high ionization component at  $v = -44 \text{ km s}^{-1}$  (cloud OVI<sub>1</sub>) has detected NV and OVI. Photoionization models with any ionization parameter would overproduce CIV at that velocity. A collisional ionization model with  $\log T \sim 5.33$  provides the best fit to the NV and OVI at  $v = -44 \text{ km s}^{-1}$ . For the blueward component at  $v = -147 \text{ km s}^{-1}$  (cloud CIV<sub>1</sub>) CIV and NV are detected, and OVI is ambiguous. A photoionization model would overproduce CIII blueward of  $-150 \text{ km s}^{-1}$ , beyond the saturated trough that may or may not be CIII 977 from this system. A collisional ionization model with  $\log T \sim 5.12$  can fit the observed CIV and NV absorption without overproducing other transitions.

It is possible to tune the metallicities of the two broad collisional components so that the wings of the Ly $\alpha$  and Ly $\beta$  lines are fit. For the  $\log T \sim 5.33$  cloud at  $v = -44 \text{ km s}^{-1}$  (cloud OVI<sub>1</sub> that produces OVI and NV absorption), this requires  $\log Z \sim -0.2$ . For the  $\log T \sim 5.12$  cloud at  $v = -147 \text{ km s}^{-1}$  (cloud CIV<sub>1</sub> that produces NV and CIV absorption), this requires a supersolar metallicity of  $\log Z \sim 1.0$ . These clouds are shown in the final, full profile plotted in Figure 1, but not as individual lines.

#### 4.1.2. Discussion

The  $z = 1.3430$  system has low ionization absorption clouds (MgII<sub>1</sub>–MgII<sub>5</sub>) that appear to have densities ( $\log n_H \sim -2$ ) and temperatures ( $T \sim 10000 \text{ K}$ ) consistent with warm ISM material (Bregman (2004), and references therein). However, the high ionization absorption is not aligned with the lower ionization absorption, indicating that it is not caused by the same clouds. Blending is a large problem with the high ionization transitions, but there is enough overlapping unblended data between the CIV and OVI doublets to allow for confirmation of our models. These high ionization clouds favor collisional ionization at  $T \sim 100000 - 200000 \text{ K}$ , which could be caused by shock heating of the region. This could be the same mechanism as the conductive interface model proposed by Fox et al. (2004). The different high ionization components show different metallicities, with the red component (cloud OVI<sub>1</sub>) having roughly the same metallicity as the lower ionization transitions ( $\log Z \sim -0.2$ ). The blue component (cloud CIV<sub>1</sub>), however, has a supersolar metallicity. This is unusual and perhaps due to ambiguities in the model, but it could also indicate a region of intense enrichment by supernovae.

This system, while just below the cutoff to be classified as a strong MgII absorber, has kinematics very similar to classic strong systems (Charlton & Churchill 1998; Churchill & Vogt 2001). It also shows a partial Lyman limit break, in contrast to the classic strong system’s full Lyman limit break. This may indicate a scenario in which this line of sight

skirts the edge of, or a sparse region of, a galaxy disk that would otherwise create a strong MgII absorption system.

Having high ionization gas in a phase that is different from the lower ionization gas is not unusual for strong or weak MgII systems (Churchill et al. 1999b, 2000b; Rigby et al. 2002; Charlton et al. 2003). When found in a strong system, the high ionization absorption usually covers similar velocities as the lower ionization absorption. It is either kinematically grouped with the low ionization gas or in a broad profile surrounding the low ionization component (Ding et al. 2004, 2003b). However, in this multiple cloud weak MgII system at  $z = 1.3430$ , the high ionization clouds are kinematically quite distinct from the low ionization clouds. There are other cases of multiple cloud weak systems showing such distinct high ionization features (Zonak et al. 2004; Ding et al. 2004). If this trend is still apparent in a larger sample, it could be very telling about the differences between multiple cloud strong and multiple cloud weak MgII systems. One example is the  $z = 1.04$  system toward quasar PG 1634 + 706 (Zonak et al. 2004). The authors of that paper found that their system had kinematically offset OVI components  $\sim 50 \text{ km s}^{-1}$  to the red and  $\sim 50 \text{ km s}^{-1}$  to the blue of the main MgII clouds. The authors suggested that their system could be related to dwarf galaxy winds. The broad OVI clouds also had a significantly higher metallicity than the MgII clouds. Our  $z = 1.3430$  system could be produced by a similar situation, though its OVI appears to be collisionally ionized, not photoionized. It is possible for winds to have a higher metallicity than that of the host galaxy (Martin 2003). These low ionization clouds could be supernova-enhanced host galaxy material, material entrained in the outflowing winds, or material in a conductive interface zone.

## 4.2. The $z = 1.3250$ System

### 4.2.1. Results

The MgII  $\lambda\lambda 2796, 2803$  for this system, shown in Figure 2 can be fit with six distinct components from  $-82 \text{ km s}^{-1}$  to  $143 \text{ km s}^{-1}$ , clouds MgII<sub>1</sub>–MgII<sub>5</sub> in Table 7 (Churchill, Vogt, & Charlton 2003). The total equivalent width of the system of  $W(2796) = 0.291 \pm 0.011 \text{ \AA}$  classifies it as a multiple-cloud, weak MgII absorber, just below the  $0.3 \text{ \AA}$  threshold for strong systems. MgI and FeII were also detected in the HIRES spectrum, while Ly $\alpha$ , Ly $\beta$ , SiII, CII, SiIII, and OVI were detected in the STIS spectrum. There is Galactic MgII 2803  $\sim 200 \text{ km s}^{-1}$  blueward of the SiIII 1207 detection, and an unidentified feature  $\sim 250 \text{ km s}^{-1}$  redward of it. It is likely that there are some unidentified absorbers blending with SiIII 1207 in the region of interest as well. It is clear that NV 1239 is at least partially blended, since NV 1243 is not detected at  $v < -180 \text{ km s}^{-1}$ . OVI 1032 is blended with

Ly $\beta$  from an OVI system at  $z = 1.3385$ , but the region at  $v > 40 \text{ km s}^{-1}$  ( $v > 200 \text{ km s}^{-1}$  at  $z = 1.3385$ ) is not affected by this blend since the corresponding Ly $\alpha$  is not detected. OVI 1038 at  $v > 0 \text{ km s}^{-1}$  is blended with the OVI 1032 line from the  $z = 1.3385$  system. Taking into account these blends, the OVI doublet can be fit with a minimum of three Voigt profile components, shown in Figure 2 and listed as clouds OVI<sub>1</sub>–OVI<sub>3</sub> in Table 7.

We first consider whether the detected CIV and OVI absorption can arise in the same phase of gas as the MgII and other lower ionization transitions. The ionization parameters of the three MgII clouds with detected FeII (clouds MgII<sub>2</sub>, MgII<sub>4</sub>, and MgII<sub>5</sub>) are all in the range  $-3.6 < \log U < -3.3$ , while upper limits can be set for the other three. With these ionization parameters, tuned to fit FeII, SiII is overproduced. Upper limits for the ionization parameters of the three clouds without detected FeII (clouds MgII<sub>1</sub>, MgII<sub>3</sub>, and MgII<sub>6</sub>) are derived such that CII, SiII, and SiIII are not overproduced. A model using these limits, given in Table 7, severely underproduces the CIV and OVI absorption, as shown by the dashed line in Figure 2.

The metallicity of the MgII clouds (MgII<sub>1</sub>–MgII<sub>6</sub>) was constrained by the partial Lyman Limit break and the Ly $\alpha$  and Ly $\beta$  profiles. Since the Lyman limit breaks of the  $z = 1.3250$  and  $z = 1.3430$  systems overlap, an iterative process was needed to co-model these two systems. For this  $z = 1.3250$  system, the Ly $\alpha$  and Ly $\beta$  profiles are best fit if clouds MgII<sub>5</sub> at  $v = 48 \text{ km s}^{-1}$  and MgII<sub>6</sub> at  $v = 143 \text{ km s}^{-1}$  have metallicities of  $\log Z \sim -0.3$ . Smaller metallicities for these two clouds are ruled out, since Ly $\alpha$  and Ly $\beta$  would be overproduced. The metallicities of clouds MgII<sub>1</sub>–MgII<sub>4</sub>, at  $v = -82, -60, -35,$  and  $-5 \text{ km s}^{-1}$ , are not constrained in this way, and so we assume that they also have metallicities of  $\log Z \sim -0.3$ . Even for extremely low metallicities we could not fit the blue edge of the Ly $\alpha$  and Ly $\beta$  profiles, and for such low metallicities the Lyman limit break constraint would be severely violated. Combined with the Ly $\alpha$  component (cloud Ly $\alpha$ <sub>1</sub> discussed below), these MgII clouds fill out the remainder of the Lyman limit break left after the  $z = 1.3430$  system was modeled. The clouds MgII<sub>2</sub> and MgII<sub>5</sub>, at  $v = -60$  and  $48 \text{ km s}^{-1}$ , were the primary contributors to the Lyman limit break, among the metal lines.

Also detected was MgI 2853 at a  $\sim 3\sigma$  level from the  $v = -5 \text{ km s}^{-1}$  cloud, MgII<sub>4</sub>. It is not fit by the low ionization clouds used to fit MgII, FeII, SiII, and CII. This may require a separate very-low ionization phase (Ding et al. 2003a). Properties of such a phase cannot be constrained by the present data.

The CIV and OVI can both be produced with three additional clouds, OVI<sub>1</sub>–OVI<sub>3</sub>, which were optimized on OVI based on the OVI Voigt profile fit described above (and shown by the dot-dashed line in Figure 2). The best fit to the low resolution CIV profiles is obtained for ionization parameters of  $\log U \sim -1.0$  for clouds OVI<sub>1</sub>–OVI<sub>3</sub>. The metallicities of all the



OVI clouds were assumed to be the same, yielding a value of  $\log Z \sim -0.3$ , based on the first red wing of the Ly $\beta$  profile. This leads to cloud sizes of 5–20 kpc. Nitrogen had to be lowered 0.8 dex, 0.5 dex, and 1.2 dex respectively from solar in our models of these three high ionization clouds to prevent overproduction of NV, which has no absorption observed. These clouds account for much of the Ly $\alpha$  and Ly $\beta$  absorption, as shown in Figure 2, however they do not fully account for the Ly $\alpha$  and Ly $\beta$  at  $-180 \leq v \leq -100 \text{ km s}^{-1}$ .

A final cloud centered at  $-137 \text{ km s}^{-1}$ , Ly $\alpha_1$ , was added to fill in the section of the Ly $\alpha$  profile that the OVI could not account for, as well as much of the Ly $\beta$  feature. The metallicity and ionization parameter of this cloud were only constrained so that there was no production of any metal-line absorption. A value of  $\log Z = -3.5$  was used in the sample model in Table 7. Due to the lack of any constraints, cloud Ly $\alpha_1$  was assumed to have an ionization parameter of  $\log U = -2.0$ . For this model, the Ly $\beta$  profile is not completely filled in if the Ly $\alpha$  profile is matched, especially on the blue wing. Either, the Ly $\beta$  is blended with unidentified lines, or a more complex model is needed. The Ly $\alpha$  also has a few sections ( $v \sim 100 \text{ km s}^{-1}$ ,  $v \sim 190 \text{ km s}^{-1}$ ) which are underproduced by the model, but they could not be fit without overproducing Ly $\beta$ . This Ly $\alpha$  cloud (Ly $\alpha_1$ ), along with the six MgII clouds in this system (MgII $_1$ –MgII $_6$ ), produces the remaining Lyman limit break absorption not filled in by the  $z = 1.3430$  system.

#### 4.2.2. Discussion

It is difficult to distinguish disk material from halo material. Inferences could be drawn from a statistically large sample, but for any one system there is no way to make a clear separation because halo clouds overlap kinematically with disk clouds. However based on the results of Charlton & Churchill (1998) and Steidel et al. (2002), we statistically can say that because of the lack of primary component, there is a low probability that this line of sight passes through any significant galaxy disk material.

The high ionization transitions in this system, in particular the OVI, are corrupted by strong blends, which makes analysis much more difficult. Still, we are able to confidently say that any high ionization gas present must be independent of the low ionization gas observed. This is very similar to what we observed in the  $z = 1.3430$  system, but again in contrast with the standard picture of strong MgII systems. Are these two systems, along with the  $z = 1.04$  system toward PG 1634 + 706 (Zonak et al. 2004), prototype members of a separate class of MgII absorber? This would be a class of multiple cloud weak absorbers with unrelated high ionization kinematics.

The MgII kinematics of the  $z = 1.3250$  system is very similar to a subsystem of the  $z = 0.9254$  absorber presented by Ding et al. (2003b) (called “System A” in that paper). Alone, System A would be classified as a multiple cloud weak MgII absorber, but it is clustered with Systems B ( $z = 0.9276$ ) and C ( $z = 0.9342$ ), a few 100 and 1000 km s<sup>-1</sup> to the red, respectively. Therefore, it is part of what has been classified as a “double” strong MgII absorber. Though the metallicity of System A ( $\log Z = 0.5$ ) is higher than our  $z = 1.3250$  system ( $\log Z = -0.3$ ), the kinematics of the MgII is very similar, suggesting a similar environment for both. The  $z = 0.9254$  system is likely to be associated with either a  $2 L_*$  spiral galaxy, or a  $0.2 L_*$  galaxy with unknown morphology. Both were found to be at the same redshift as the absorber, and at about equal impact parameters ( $43 h^{-1}$  kpc). System B is identified with an  $L_*$  galaxy at an impact parameter of  $38 h^{-1}$  kpc. The whole situation is suggestive of a group of galaxies with lines of sight at large impact parameter through the outskirts of the galaxies. This could be a hint of the galaxy type and environment of the  $z = 1.3250$  system, for which we have no direct information.

However, not all is the same between System A and the  $z = 1.3250$  absorber. System A has very strong NV absorption, whereas our system has so little that an abundance pattern adjustment is required to account for its deficiency. While there have been many papers which discuss strong nitrogen underabundances in DLAs, many of those focus on systems with metallicities lower than our system ( $-2 < \log Z < -1$  compared to our  $\log Z = -0.3$  (Pettini 2003)). Our system is apparently different from such DLAs and from dwarf galaxies, which are also nitrogen deficient, but have low metallicity as well (Mateo 1998). This may suggest an enrichment scenario which is only primary, however coverage of oxygen transitions would be required to be able to determine this.

A more interesting (though speculative) hypothesis is that our  $z = 1.3250$  system and System A of Ding et al. (2003b) represent the absorption features of the tidal tails and debris from interacting galaxies. Due to multiple interactions in a group, material may be dispersed, with some regions collapsing to form star clusters, tidal dwarf galaxies and other gaseous concentrations. Should our line of sight pass through such a region, pockets of higher density would be randomly crossed, giving absorption profiles with many smaller features, but no main feature. Such a circumstance was suggested by the group environment known for the PG 1206 + 459 absorbers (Ding et al. 2003b), but in our case, there is much less supporting evidence. Unless the line of sight fell along one of the tails, multiple interactions would be needed to produce the structures with a large spread in velocity. Without an image deep enough to resolve the galaxy/galaxies associated with this absorber, we cannot test this speculation.

There is also a small amount of MgI absorption observed for the  $v = -5$  km s<sup>-1</sup> cloud,

which our models cannot account for. This absorption cannot be produced in the same phase as the MgII, and can only be explained by an additional, very-low ionization phase at the same velocity. One way to create a phase like this is to have a cloud with a very small Doppler parameter, placing the MgII on the flat part of the curve of growth, while MgI is on the linear part (Ding et al. 2003a). Thus, the MgII associated with the MgI does not have to be the strongest observed, as in this case. This would imply that the MgI forms in smaller, dense regions of the MgII cloud, so that a single line of sight may only pass through one such region.

### 4.3. The $z = 1.0480$ System

#### 4.3.1. Results

The MgII  $\lambda\lambda 2796, 2803$  profiles for the  $z = 1.0480$  system are fit with seven Voigt profile components, clouds MgII<sub>1</sub>–MgII<sub>7</sub>, in two separate subsystems at  $\sim 0$  km s<sup>-1</sup> and  $\sim -90$  km s<sup>-1</sup> (Churchill, Vogt, & Charlton 2003). MgI 2853 and FeII 2600 are also detected in the HIRES spectrum. In the STIS spectrum, the Ly $\alpha$  profile is significantly extended blueward of the two subsystems. The SiII and CII profiles have roughly the same shapes as the MgII  $\lambda\lambda 2796, 2803$ , as does the SiIII, but the latter is contaminated by an unknown blend (probably Ly $\alpha$  at  $z \approx 1.0325$ ). We will consider the possibility that the SiIII 1207 at  $v = -186$  km s<sup>-1</sup> is a detection rather than a blend, and that it produces Ly $\alpha$  centered at that velocity. The SiIV 1394 is blended with Galactic MgI 2853, but the SiIV 1403 is detected from the subsystem at  $\sim 0$  km s<sup>-1</sup>. The NV  $\lambda\lambda 1239, 1243$  was also covered in the STIS spectrum, but it was not detected. Finally, CIV was covered, but not detected in a low resolution optical spectrum from Palomar (Steidel & Sargent 1992).

The ionization parameter was first constrained for the seven MgII clouds, assuming that MgII, FeII, and MgI are present in the same phase. The ionization parameters found for these clouds, MgII<sub>1</sub>–MgII<sub>7</sub> in Table 8, ranged from  $\log U = -4.1$  to  $\log U = -3.6$  (see Table 8). This conclusion is nearly independent of metallicity constraints, which are discussed below. For clouds MgII<sub>1</sub>, MgII<sub>3</sub>, and MgII<sub>7</sub>, those for which FeII is not detected, these  $\log U$  values can be taken as lower limits. For these values of  $\log U$ , the SiIV is not fully produced. Since the determined value was a lower limit, the ionization parameter of cloud MgII<sub>3</sub>, at  $v = -23$  km s<sup>-1</sup>, could be raised to  $\log U = -2.5$  so that it does produce the SiIV at that velocity. However, an additional phase would still be required to produce the SiIV 1403 centered at  $v \sim 6$  km s<sup>-1</sup> (recall that the SiIV 1394 is contaminated by a blend at this velocity).

We consider photoionization and collisional ionization for the phase of gas that produces the SiIV absorption at  $v \sim 6 \text{ km s}^{-1}$ . If it is photoionized, either the SiIII or the CIV would be drastically overproduced. Such a case, for which a model needs to dominantly produce a particular ionization stage, suggests collisional ionization at a higher temperature. Using SiIV, SiIII, CII, and SiII, the temperature was found to be  $\log T \sim 4.74 \text{ K}$ . The parameters for this collisionally ionized cloud, SiIV<sub>1</sub>, are listed in Table 8.

The possible SiIII absorption at  $v = -186 \text{ km s}^{-1}$  is centered on a region of the Ly $\alpha$  profile that could be interpreted as a separate component (from  $\sim -250$  to  $-130 \text{ km s}^{-1}$ ). It is possible to fit this region of the Ly $\alpha$  profile and the SiIII absorption at  $v = -186 \text{ km s}^{-1}$  with a single cloud, SiIII<sub>1</sub>, with  $\log U \sim -2.1$  and  $\log Z \sim -1.4$ . For this metallicity, values of  $\log U$  much smaller than  $-2.1$  are not possible because lower ionization transitions are not detected at this velocity. This model component was considered because of the small amounts of flux apparently detected in the Ly $\alpha$  profile at  $v \sim -250$  and  $v \sim -140 \text{ km s}^{-1}$ . If this is valid, another Ly $\alpha$  component, Ly $\alpha$ <sub>1</sub>, without corresponding detected metal line transitions, would have to be added at  $v \sim -266 \text{ km s}^{-1}$ . This component, assuming the same metallicity as the SiIII component, could not have an ionization parameter larger than  $\log U \sim -3.0$  without overproducing SiIII absorption. If the possible SiIII absorption at  $v = -186 \text{ km s}^{-1}$  is the result of a blend, there is even more flexibility in fitting the Ly $\alpha$  at  $v < -130 \text{ km s}^{-1}$ . In either case, it is clear additional components are needed to fit the Ly $\alpha$ .

To simplify the process of constraining the metallicity of the clouds in this system, all of the MgII clouds (MgII<sub>1</sub>–MgII<sub>7</sub>) were initially assumed to have the same value. Based on the Lyman limit break, which is dominated by the contribution of the HI in the MgII clouds, the metallicity of these clouds was  $\log Z \sim -0.7$ . The metallicity of the SiIV cloud (SiIV<sub>1</sub>) was based on fitting the red wing of the Ly $\alpha$  profile. The Ly $\alpha$  in this region, from  $v \sim 80 \text{ km s}^{-1}$  to  $v \sim 120 \text{ km s}^{-1}$  was clearly underproduced by the MgII clouds, shown as the dashed line in Figure 3. To fit the wing, the metallicity of the collisionally ionized SiIV cloud (SiIV<sub>1</sub>) was found to be  $\log Z \sim -1.4$ . For simplicity, in our tabulated model, also displayed in Figure 3, the SiIII and Ly $\alpha$  clouds (SiIII<sub>1</sub> and Ly $\alpha$ <sub>1</sub>) were taken to have the same metallicity as this SiIV cloud (SiIV<sub>1</sub>).

An alternative model is one in which the Ly $\alpha$  absorption is produced primarily in a single, broad component. This model assumes that the apparent detected flux seen at  $v \sim -250 \text{ km s}^{-1}$  and  $v \sim -140 \text{ km s}^{-1}$  is just the result of correlated noise in the data. In this case, the excess Ly $\alpha$  absorption, not produced by the MgII clouds, can be fit by a single cloud centered at  $v \sim -98 \text{ km s}^{-1}$ , with  $\log N(\text{Ly}\alpha) \sim 16.3 \text{ cm}^{-2}$  and  $b \sim 75 \text{ km s}^{-1}$ . However, this cloud is constrained not to produce any detectable absorption in any of the

covered transitions. For any  $\log U < -1.0$ , this would require extremely low metallicities, i.e.  $\log Z < -2.7$ . Any broad, high ionization phase for this system is constrained in this way as well. It seems more likely that the Ly $\alpha$  absorption arises in the several narrower clouds, as discussed above.

#### 4.3.2. Discussion

The  $z = 1.0480$  system along this line of sight is very interesting, as it would appear to be a classic strong MgII system, with the exception that it is CIV deficient. Churchill et al. (1999a) proposed that CIV is produced by a corona phase around the host galaxy, based upon the correlation between the equivalent width of the CIV and the velocity spread of the MgII clouds. In that model, the outermost MgII clouds were high velocity clouds associated to the same star-forming processes that supported the corona. Does our lack of CIV detection indicate that this galaxy is not undergoing star formation? There is also some evidence that CIV deficient galaxies tend to be reddish, which is indicative of gasless, older host galaxies, perhaps elliptical (Churchill et al. 2000a). On the other hand, the CIV deficient system at  $z = 0.6600$  toward the quasar PG 1317+274 is likely to be related to a spiral galaxy (Steidel et al. 2002), although it is a spiral with a reddish color ( $B-K=3.84$ ). Recently, Ding et al. (2004) have suggested that CIV deficiency is a general feature of systems without a corona, and that there are a variety of reasons for a lack of corona, meaning that many different morphologies could cause CIV deficient absorption.

For our system, one possible explanation for the CIV deficiency is that the host galaxy could be at a rather large impact parameter ( $d \geq 30 h^{-1}$  kpc). Beyond the corona (which could be contained in the inner disk), little or no CIV would be observed. Conversely, if all the gas was in a particularly highly ionized corona, the CIV would be pushed into higher ionization states. This would be observable as very strong OVI absorption, however OVI was not covered by our spectrum. This gas would be constrained not to produce any CIV or NV absorption. This could be due to collisional ionization, as is found in the  $z = 1.3430$  system, though at even higher temperature, to limit the NV and CIV absorption. Another explanation could be a low metallicity corona, or a complete lack of a corona. The low metallicity case could be investigated with observations of higher order transitions in the Lyman series. Although the kinematics are suggestive of a spiral, in the absence of direct information about the galaxy host, this could be an early type galaxy. A deeper image of the area around the quasar with spectroscopic confirmation to detect the host of this system would be very helpful in ruling out possibilities. High resolution spectral observations covering OVI absorption for this system would also be useful, though this would be a difficult

observation because the flux in that region is greatly reduced due to the Lyman limit breaks of the  $z = 1.3430$  and  $z = 1.3250$  systems.

The Ly $\alpha$  absorption found in this system can be explained with either a single, broad component, or with multiple narrower components. We tentatively favor a multiple component explanation because of the alignment between the Ly $\alpha$  absorption and the SiIII components. However, a very low metallicity, broad Ly $\alpha$  component is possible. Were this the case, this system would be similar to the  $z = 0.9902$  system toward PG1634 + 706. In that case, a large, low metallicity halo was proposed to be responsible for most of the Ly $\alpha$  absorption. It is tempting to say that these are similar systems, however either explanation is possible.

#### 4.4. The $z = 0.7290$ System

##### 4.4.1. Results

The 0.7290 system is a multiple-cloud, weak MgII absorber with a total  $W_r(2796) = 0.240 \pm 0.008 \text{ \AA}$ . In the HIRES spectrum MgII, MgI, and FeII absorption are detected, and can be fit by five distinct, narrow Voigt profiles ( $3 < b < 5 \text{ km s}^{-1}$ ), ranging in velocity from  $-82 \text{ km s}^{-1}$  to  $67 \text{ km s}^{-1}$ , clouds MgII<sub>1</sub>–MgII<sub>5</sub> in Table 9 (Churchill, Vogt, & Charlton 2003). CII 1335 is detected in the STIS spectrum, but AlII 1671 cannot be separated from the noise. SiIV 1403 is not detected, providing a limit on SiIV despite the features in the confused region of the spectrum around SiIV 1394. Most importantly, CIV  $\lambda\lambda 1548, 1551$  is not detected, with  $W_r(1548) < 0.010 \text{ \AA}$  at a  $3\sigma$  level. For  $b = 4 \text{ km s}^{-1}$ , this corresponds to  $\log N(\text{CIV}) = 12.4 \text{ cm}^{-2}$ . The detected transitions, along with the region covering CIV  $\lambda\lambda 1548, 1551$ , are shown in Figure 4. A Lyman limit break is not detected for this system, however caution is in order because it would appear in the first dozen pixels of the FOS spectrum, which may be too noisy to be sure there is no feature there.

A single, low ionization phase was used to fit all the observed transitions. For simplicity, we assumed that all clouds had the same metallicity. Based on the lack of a Lyman limit break,  $\log N(\text{HI}) < 16.5 \text{ cm}^{-2}$  and a limit of  $\log Z \geq 0.6$  is placed on the metallicity. The ionization parameter can be constrained by the FeII 2600, assuming solar abundance pattern. Using a metallicity of  $\log Z \sim 0.7$ , clouds MgII<sub>2</sub>–MgII<sub>4</sub>, at  $v = -64, -9, \text{ and } 12 \text{ km s}^{-1}$ , would have ionization parameters  $-4.4 < \log U < -4.1$ . Cloud MgII<sub>1</sub>, at  $v = -82 \text{ km s}^{-1}$ , would have an ionization parameter  $-3.2 < \log U < -2.9$ . Cloud MgII<sub>5</sub>, at  $v = 67 \text{ km s}^{-1}$ , is only observed in MgII, and so the ionization parameter for it can only be restricted to a lower limit of  $\log U \leq -2.5$ , based on CIV production. (The feature to the red of FeII 2600

is MgI 2853 from the  $z = 0.5764$  system.) These values of  $\log U$  are consistent with the observed MgI 2853 absorption, but they severely underproduce CII 1335. An increase of the carbon abundance of between 0.5 and 2.0 dex was required to bring the model into agreement with the data. Alternatively, we could increase  $\log U$  to bring the CII 1335 into agreement, however, this would both overproduce CIV and require a large increase in the iron abundance.

A  $\log Z = 0.7$  model for the low ionization phase is listed in Table 9. The sizes of these weak clouds (MgII<sub>1</sub>–MgII<sub>5</sub>) are extremely small ( $\lesssim 1$  pc), and they are quite cold due to their high metallicities. To pass through five such clouds along a single line of sight would imply a large covering factor and/or an unusual geometry. Because of these extreme properties and because the determination of the lack of Lyman limit break from the FOS data was so uncertain, we consider an alternative model with  $\log Z = -1.0$ . This model is problematic, because not only is there a Lyman limit break created, but it also overproduces CIV and underproduces FeII, even at the same ionization parameters as the  $\log Z = 0.7$  model. Should the carbon abundance adjustment be decreased, overproduction of CIV would still occur, and CII would then be underproduced. We find it unlikely that this model is correct.

The most striking thing about this system is the absence of detected CIV. As just described, it is consistent with the low ionization transitions to have negligible CIV produced in the low ionization phase, regardless of metallicity. The lack of detected CIV also constrains the properties of any possible broad, high-ionization phase. Such a phase would have either extremely low metallicity or a high ionization parameter. The former could be diagnosed by high resolution coverage of Ly $\alpha$  and the latter by NV and OVI profiles.

#### 4.4.2. Discussion

The  $z = 0.7290$  system is a multiple cloud weak MgII system, but is similar to the  $z = 1.0480$  strong MgII system in the respect that it has no detected CIV absorption. In this case, CIV is covered by the STIS spectrum, which has a much greater sensitivity than the ground-based data used in the  $z = 1.0480$  system, and SiIV is not detected either. This system has many of the same properties as the  $z = 0.6600$  system toward CSO 873 presented by Ding et al. (2004). Again, we consider whether that the lack of the CIV absorption is due to galaxy structure, ionization, or low metallicity.

We inferred a very high metallicity for the low ionization phase. This may suggest that a low metallicity corona is highly unlikely. However, our high metallicity determination ( $\log Z \geq 0.6$ ) is based almost entirely on the lack of a Lyman limit break, which would

only be observed at the very end of the FOS spectrum. This introduces uncertainty into our conclusion. If this high metallicity is correct, though, it is very significant. Single cloud weak MgII clouds have been shown to have metallicities greater than 0.1 solar (Rigby et al. 2002) and in many cases greater than solar (Charlton et al. 2003), but it has been suggested that multiple cloud weak MgII systems are completely different objects, with much lower metallicities (Zonak et al. 2004; Rosenberg et al. 2004). Also, single cloud weak systems commonly have CIV detected, in the redshift range of  $0.5 \leq z \leq 1$  (Rigby et al. 2002). The single cloud weak MgII absorbers are a different class of absorbers than strong MgII absorbers, representing high metallicity regions that could fully account for the Ly $\alpha$  forest with  $\log N(\text{HI}) > 15.8 \text{ cm}^{-2}$ . Our view of the nature of the structures in which they arise could be greatly influenced by the existence of multiple cloud versions of single cloud weak absorbers.

A consequence of the high metallicity we have found is that these clouds have low temperature. This is not because they are dense, but is a direct result of the high metallicity cooling the clouds, making them very different from the MgI phase of the  $z = 0.99$  system toward PG 1634+706 presented by Ding et al. (2003a). In that system, a very-low metallicity phase was required to explain the broad Ly $\alpha$  profile, weak CIV, and lack of detected NV and OVI. The authors suggested the phase could be a galactic halo or a diffuse medium in an early type galaxy, but they had no direct galaxy information. In our case, we know that our absorption system is associated with a red face-on barred spiral galaxy (approximately SBa) at  $36 h^{-1}$  kpc. Without coverage of the Ly $\alpha$ , NV or OVI, we can only speculate that a similar broad component could exist, but if it does we would know that an elliptical could produce such a signature. As with the  $z = 1.0480$  system, we note that several types of CIV deficient systems could exist, with the common element being the lack of a traditional CIV corona.

An oddity of this system is the abundance enhancement of carbon that is required to fill out the observed CII absorption. Gehrz et al. (1998) presented results indicating that novae from carbon-oxygen (CO) white dwarfs would produce excesses in carbon and silicon. It would be interesting to have SiII coverage for this system, to see if abundance increase is required for that as well. This could indicate novae activity resulting from low-mass ( $\lesssim 1.2 M_{\odot}$ ) white dwarfs accreting and detonating.



## 4.5. The $z = 0.5764$ System

### 4.5.1. Results

This system is a very strong Mg II absorber, with  $W_r(2796) = 0.902 \pm 0.002 \text{ \AA}$  (Churchill & Vogt 2001). In addition to the Mg II doublet, Mg I, Ca II, and Ti II were detected in the Keck I/HIRES spectrum. These profiles could be fit with a minimum of four Voigt profile components, with a velocity range of  $-31 \text{ km s}^{-1}$  to  $77 \text{ km s}^{-1}$  (Churchill, Vogt, & Charlton 2003) (see clouds Mg I<sub>1</sub>–Mg I<sub>3</sub> and Mg II<sub>1</sub> in Table 10, which come from the fit). In the *HST*/STIS spectrum, C IV  $\lambda\lambda 1548, 1551$ , Si II 1527, Al II 1671, Fe II 1608, Al III 1855, and Al III 1863 were detected. The velocity range for the C IV was greater than that for the lower ionization gas, with a component at  $-95 \text{ km s}^{-1}$ . The detected transitions from HIRES and STIS are shown in Figure 5. The Ly $\alpha$  was covered only in a low resolution ( $R \sim 1300$ ) *HST*/FOS spectrum, obtained in spectropolarimetry mode (Koratkar et al. 1998). It gives only a rough measure of  $W_r(1216)$  and a tentative indication of the profile shape. It is unclear whether the profile indicates a damped Ly $\alpha$  absorber, or whether it can be better fit with multiple components, with lower HI column densities (Rao & Turnshek 2000).

The Mg II  $\lambda\lambda 2796, 2803$  and Si II 1527 transitions are saturated and any subcomponent structure cannot be discerned due to blending. However, the Al II 1671 and the Al III  $\lambda\lambda 1854, 1862$  transitions are not saturated, and so provide a constraint on these transitions. The very-low ionization transitions, Mg I, Fe II, Ca II, and Ti II, also show some kinematic structure. Therefore, we use the Voigt profile fit to the Mg I 2853, clouds Mg I<sub>1</sub>–Mg I<sub>3</sub>, as a starting point for the photoionization models. A very-low ionization phase, with  $-8.2 < \log U < -7.7$ , can be used to fit the Mg I and Ca II in cloud Mg I<sub>2</sub> at  $v = -9 \text{ km s}^{-1}$ , but it underproduces Ti II and Fe II. To adequately fit the Ti II profile would require the titanium abundance to be elevated by  $\sim 1.9$  dex relative to magnesium and calcium. Dust depletion is known to reduce titanium and calcium absorption (Savage & Mathis 1979). Were this taken into account as well, the abundance pattern adjustments would have to be even further increased. For the assumed range of ionization parameters and a metallicity of  $\log Z = -1.9$  (from the low ionization phase, as described below), the cloud sizes range from 0.0008 to 0.018 pc. For higher values of the metallicity, the titanium abundance elevation would have to be even more extreme. The Fe II was adequately fit with an abundance elevation of  $\sim 1.2$  dex. Any variation in ionization parameter or metallicity would only serve to require a greater abundance pattern shift. Figure 5 shows the contribution of the very-low ionization phase (clouds Mg I<sub>1</sub>–Mg I<sub>3</sub>) to the Mg II, Fe II, and Si II as a dotted line, showing the need for a low ionization phase.

The low ionization phase was able to be constrained by the required production of the

saturated transitions, but more importantly by the two AlIII transitions. For simplicity, we assumed three components (clouds SiII<sub>1</sub>–SiII<sub>3</sub>) centered on the three very-low ionization phase components, and found a plausible fit to the SiII 1527 profile with the minimum values of the column densities. These components could only be constrained very loosely, using the requirements that the MgII profile be filled, and the AlII, FeII, and CaII not be overproduced. Attempting to fit the components to the FeII profile resulted in overproducing CaII to a greater degree than FeII was underproduced by the very-low phase, prompting us to vary the abundance of iron in that phase.

Because of saturation effects, specific values of constraints should be viewed with caution. For example, if the SiII 1527 column densities were larger, then  $\log U$  would be constrained to be higher. Also, the model fits to the AlII 1671 and MgII  $\lambda\lambda$ 2796, 2803 are not consistent with the data, suggesting additional abundance parameter adjustments and/or a more complex phase structure. It may be possible to resolve this by adjusting the silicon abundance in the low ionization phase, however.

Nonetheless, the essential conclusion concerning the low ionization phase is that most of the CIV absorption cannot be produced by these same clouds. This is not true for regions of velocity coinciding with  $v = -9$  and  $v = 16$  km s<sup>-1</sup> clouds (SiII<sub>2</sub> and SiII<sub>3</sub>): these can be adequately fit by the low ionization phase; when the ionization parameter is constrained by SiII and AlIII, the CIV is also consistently produced.

Cloud MgII<sub>1</sub>, at  $v = 77$  km s<sup>-1</sup>, is able to produce MgII and CIV at that velocity in a single phase having an ionization parameter of  $-2.3 < \log U < -2.2$ . However, an alternative model with two phases is also possible. With no additional unblended low ionization transitions, we will refrain from speculating further on the existence of more than one phase in this cloud.

Using the FOS data, and assuming that the observed Ly $\alpha$  profile was indeed a single, damped Ly $\alpha$  (DLA) feature, we can consider the metallicity of the very-low ionization clouds, MgI<sub>1</sub>–MgI<sub>3</sub>. The metallicity constraint is also subject to uncertainties due to saturation, but we can consider our derived value as a lower limit, since we fit the SiII 1527 with the minimum column densities that were consistent with its profile. We found that the metallicity in the very-low ionization phase was constrained to be  $-2.0 < \log Z < -1.8$ , with a best fit at  $\log Z = -1.9$ , which arises from the slight variations in absorption strengths between transitions caused by varying metallicity. This effect happens in the optically thick regime.

Due to the narrow range of the velocity distribution of the low ionization gas, we were unable to model the Ly $\alpha$  profile as multiple individual components, as suggested in Rao & Turnshek (2000). It seems more likely that the Ly $\alpha$  is dominated by a single cloud, or by a

few clouds very close together in velocity space.

A higher ionization phase is needed to produce the CIV absorption in this system, for the main reason that the CIV  $\lambda\lambda 1548, 1551$  profiles have absorption lying at both higher and lower velocities than the low ionization profiles. Since CIV is the only high ionization transition covered, the only constraint on its ionization parameter is the non-detection of low ionization transitions at some velocities. This restricts the ionization parameter to  $\log U \geq -1.8$ . A plausible model, including clouds CIV<sub>1</sub>–CIV<sub>5</sub> with  $\log U = -1.8$  is summarized in Table 10.

#### 4.5.2. Discussion

This DLA system was difficult to model, due to the saturation in the MgII transitions, and the complex structure in the MgI transition. It is unlikely that our solution is unique, but we are still able to draw general conclusions from our chosen model and our other failed possibilities. It is clear that two separate ionization phases are required to produce the observed MgI, MgII, and SiII. Even with these extra phases, large abundance pattern variations are needed to account for the TiII absorption.

Having an extra very-low ionization phase is consistent with other observations of DLAs. DLA systems have been observed to have molecules (Ge, Bechtold, & Kulkarni 2001; Ledoux et al. 2002, 2003), which indicates a very cold, high density environment, consistent with a small, very-low ionization region. Narrow velocity widths would be expected from such a cold phase of gas. Lane et al. (2000) present a DLA system with a very narrow velocity width in one of the components of the 21 cm absorption, consistent with the Doppler parameters in our models of the very low ionization phase of the  $z = 0.5764$  system. The sizes that we have estimated from our models are as small as  $\sim 150$  AU, which at first may seem remarkable. However, it is known, from a variety of observational techniques, that there exists significant structure down to scales of 100 AU in the interstellar medium of the Milky Way (Andrews, Meyer, & Lauroesch 2001; Meyer & Lauroesch 1999; Watson & Meyer 1996; Meyer & Blades 1996; Frail et al. 1994). It is interesting to note that, in the absence of pressure balance, there is still no clear explanation for the small scale clumping in the Milky Way (Elmegreen 1997; Heiles 1997; Walker & Wardle 1998). In terms of small scale structure in extragalactic absorbers, Ding et al. (2003a) found similar ones in the strong MgII absorber at  $z = 1.0414$  in the PG 1634 + 706 line of sight.

The CIV absorber in this system is weaker relative to the MgII than is expected for a classic, strong MgII system (Churchill et al. (2000b); although those authors were work-

ing with a very small sample, which should be taken into consideration). The CIV does not appear to be associated with lower ionization gas, even just based on the stark velocity differences between the observed absorption in each. This is consistent with the DLA absorption being due to a contained region within a larger structure.

If the line of sight did not happen to pass through this contained region, the system would have the same absorption properties as an ordinary MgII absorber. This idea is supported by the fact that the candidate galaxy believed to be associated with this absorber is at a very small impact parameter ( $d = 5.1 h^{-1}$  kpc). It is interesting that the CIV absorption in this DLA is weaker than any other DLA's in the small sample of Churchill et al. (2000b), especially because this is associated with a potential elliptical galaxy. In some cases the CIV absorption in a DLA could be enhanced by the contributions from very high column density MgII clouds, however, in this case the effect of this enhancement is not large.

## 5. System Summary

We present the results from our photoionization and collisional ionization modeling of five intervening quasar absorption line systems along the line of sight toward the quasar PG 0117 + 213. Starting with the highest redshift system, we analyzed the absorption features of the  $z = 1.3430$ ,  $z = 1.3250$ ,  $z = 1.0480$ ,  $z = 0.7290$ , and  $z = 0.5764$  absorption systems.

- The three phase  $z = 1.3430$  system is a multiple cloud weak MgII absorber which had low ionization phase properties similar to many strong MgII absorbers. The high ionization components were found to be unrelated to the low ionization gas due to the differences in their kinematics. In addition, both high ionization components are found to be collisionally ionized, with different metallicities, one of which varies significantly from the metallicity of the low ionization gas. A broad, low metallicity Ly $\alpha$  component was needed to fill in the wings of the Ly $\alpha$  absorption. The nature of the host galaxy is not known, but we suggest that this system could be produced in the outskirts of a spiral disk, or in a dwarf galaxy.
- The three phase  $z = 1.3250$  system is a multiple cloud weak MgII absorber as well, but its components are spread out in a distribution similar to what we might expect from an elliptical galaxy, or a spiral with no disk gas contribution (Charlton & Churchill 1998). High ionization OVI gas was seen over the same range as the low ionization gas, but again it was found not to be related to the lower ionization transitions. This system

is strong in CIV absorption, but has very weak NV absorption, requiring a significant nitrogen abundance pattern shift from solar. This system kinematically suggests an elliptical galaxy or lack of disk gas component, but it would be an exception to the possible tendency for red galaxies to be CIV deficient (Churchill et al. 2000b). On the other hand, some lines of sight through spiral galaxies in a statistical sample (those with weak absorption contributions from the disk) would have kinematics consistent with the  $z = 1.3250$  system as well (Charlton & Churchill 1998).

- The four phase  $z = 1.0480$  system is a CIV deficient strong MgII system. With only a potential host candidate in the field, we can only say that the kinematics are consistent with a spiral galaxy. However, the CIV deficiency suggests a highly ionized or sparse corona, or even the absence of a corona, such as is expected for an elliptical galaxy.
- The single phase  $z = 0.7290$  system is a multiple cloud weak MgII system that has components kinematically spread out as could be expected for an elliptical galaxy. However, the galaxy host is known to be a very red, barred spiral galaxy in the optical images of the field. This is still consistent with the fact that the absorber is CIV deficient, suggesting that the corona is weak or absent. This absorber may be a typical CIV deficient system, although we found it to possibly have supersolar metallicity with unusually small, low ionization cloud sizes.
- The three phase  $z = 0.5764$  system is a damped Ly $\alpha$  absorber, which is possibly produced by a candidate galaxy at a small impact parameter ( $5.1 h^{-1}$  kpc), which is very red ( $B-K= 4.00$ ). A separate very-low ionization phase is required to produce the observed absorption in the very-low ionization species. This system required an abundance pattern adjustment to account for all low ionization species observed (CaII, MgII, FeII, and TiII). CIV absorption is observed from this galaxy, but some of it cannot be related to the lower ionization gas due to its non-coincident velocity range. This is consistent with the idea that a DLA has low ionization absorption arising from a small region within a larger, somewhat unrelated structure.

## 6. Conclusion

We think of the Milky Way Galaxy as a typical spiral galaxy, with a structured multi-phase interstellar medium. The Milky Way also has a highly ionized corona, a few kiloparsecs thick around the disk, which produces broad absorption features in CIV, NV, and OVI (Savage et al. (2000), and references therein). These broad features do often have component structure, but the structure is usually restricted to the same velocity range as that of the

low ionization absorption. Most giant galaxies in the nearby universe are spirals, and there is also an absorption cross section presented by early type galaxies. Furthermore, there is a non-negligible cross section of dwarf galaxies, which presumably produce some absorption. There are five MgII absorption systems along the quasar PG 0117 + 213 line of sight, which are presumably produced by a random, but small, sampling of galaxies with redshifts ranging from  $z = 0.5764$  to  $z = 1.3430$ . We conclude with a discussion of how these five systems compare to the absorption seen looking through the Milky Way, and how they may resemble or differ from other kinds of absorbing structures that we see in the nearby universe.

Three of the MgII absorbers in this study are classified as multiple cloud weak MgII absorption systems. These absorbers are about two-thirds as common as strong MgII absorbers (Churchill et al. 1999b). The cross section presented by their hosts must then be significant, about two-thirds of that presented by the luminous galaxies that produce the strong MgII absorption. Because the equivalent width division at  $0.3 \text{ \AA}$  is arbitrary, we would expect some of these multiple cloud weak MgII systems are simply less extreme versions of strong MgII absorbers, which are associated with giant galaxies. Indeed, the  $z = 0.7290$  system toward PG 0117 + 213 is found to be associated with a  $\sim 3 L_K^*$  face on SBa galaxy at an impact parameter of  $36 h^{-1} \text{ kpc}$  (Churchill et al. 1996). This distance is close to the boundary of  $38 h^{-1} \left(\frac{L_K}{L_K^*}\right)^{0.15} \text{ kpc}$ , within which strong MgII absorption should occur (Steidel 1995). This absorber is a very red galaxy, and a CIV deficient system as well (which Churchill et al. (2000a) suggests is an indicator of early type galaxies, low star formation rate, or a long time since the last episode of star formation).

The other two multiple cloud weak MgII absorbers at  $z = 1.3430$  and  $z = 1.3250$  are presently too distant for the galaxy properties to be directly explored. The  $z = 1.3250$  system has kinematics similar to the  $z = 0.7290$  system, tempting us to say that the former is a very red galaxy, like the latter, and possibly an early type galaxy. However, the  $z = 1.3250$  system also has strong OVI and CIV absorption, loosely covering the same range as the low ionization absorption, and it is not CIV deficient. Perhaps some selected lines of sight through the Milky Way disk would look like this.

The  $z = 1.3430$  system is different from the  $z = 1.3250$  system in that it has a kinematically dominant component in the low ionization absorption, perhaps suggestive of a disk. Additionally, the  $z = 1.3430$  system has broad absorption in the high ionization gas that is quite kinematically unrelated to the low ionization gas. Zonak et al. (2004) have discussed the possible absorption signature of dwarf galaxies and their winds, and their possible relation to multiple cloud weak MgII systems. Dwarf galaxies must present some significant absorption cross section, and multiple cloud weak MgII absorbers could be their signature in some cases. Both the  $z = 1.3250$  and the  $z = 1.3430$  systems could fall in this category.

Generally, the three multiple cloud weak MgII absorbers along this PG 0117 + 213 line of sight illustrate the idea that there is likely to be more than one type of origin for this class of system.

The absorption from the  $z = 0.5764$  DLA system could be consistent with what would be expected from some lines of sight through the Milky Way Galaxy. However, this system is believed to be related to a very red galaxy at a relatively low impact parameter. The CIV absorption appears to be unrelated to the gas producing the DLA, but it is still substantial for a very red galaxy, many of which are CIV deficient (for example, our  $z = 0.7290$  system). On the other hand, the CIV absorption is relatively small compared to that produced by other DLAs (Churchill et al. 2000b). It will be important to analyze the kinematics of CIV relative to MgII as the sample of DLA systems studied at high resolution in multiple transitions grows.

The  $z = 1.0480$  system could be a fairly standard case of a strong MgII absorber that is CIV deficient. The possible candidate galaxy has an impact parameter of  $22.7 h^{-1}$  kpc, which is well within the boundary of  $38 h^{-1} \left(\frac{L_K}{L_K^*}\right)^{0.15}$  kpc for strong MgII absorption. This could imply that this system is an early type galaxy (elliptical or spiral with little star formation), though this is by no means definite.

As it turns out, none of the five PG 0117 + 213 MgII absorbers give the absorption signature expected for a combination of a disk, gaseous corona, and occasional high velocity clouds like we see from the Milky Way Galaxy. However, not all absorption systems at  $z \sim 1$  are so different from the expected signature of a spiral galaxy. In a couple of strong MgII absorbers (e.g. PG 1206 + 459 at  $z = 0.9276$  (Ding et al. 2003b) and PG 1248 + 401 at  $z = 0.7729$  (Ding et al. 2004)), the absorption features in high ionization gas do resemble coronae that kinematically encompass the dominant low ionization features. In some of the PG 0117 + 213 systems studied here, and in some other systems at  $z \sim 1$ , it also seems that "high velocity clouds" are producing both low and high ionization absorption (Churchill et al. 2000b). It will be of interest as data sets grow to study whether there is an evolution of the properties of high velocity clouds.

High resolution coverage of a variety of transitions for the five PG 0117 + 213 absorption systems provided information about several classes of absorbers: multiple-cloud weak MgII, CIV-deficient, and damped Ly $\alpha$ . In addition to these classes, the MgII absorber population at  $z = 1$  includes single-cloud weak MgII absorbers and traditional spiral galaxies with disks and coronae. Although they share some elements in common, we have seen that there is substantial variation in the absorption properties within a class. We plan a study of a larger sample of  $\sim 100$  MgII absorbers covering many key transitions with high resolution is feasible, using archival *HST*/STIS data in conjunction with ground-based data, when available. With

a sample of that size, it will be possible to have  $> 10$  objects within each class, which will allow separation of some classes into sub-classes, and more specific connections of other classes to physical processes and/or to morphologies of luminous hosts.

The authors would like to thank Buell Jannuzi for providing them with an early release of the STIS spectrum, and Sandhya Rao and Anuradha Koratkar for help with interpretation of the FOS spectrum. Special thanks to Michele Crowl for her careful proofreading. This research was funded by NASA under grants NAG 5-6399, NNG04GE73G, and HST-GO-08672.01-A, the latter from the Space Telescope Science Institute, which is operated by AURA, Inc., under NASA contract NAS 5-26555; and by NSF under grant AST-04-07138. JRM was partially funded by the NSF REU program.

## REFERENCES

- Andrews, S. M., Meyer, D. M., & Lauroesch, J. T. 2001, *ApJ*, 552, L73
- Bahcall, J. N., et al. 1993, *ApJS*, 87, 1
- Bahcall, J. N., et al. 1996, *ApJ*, 457, 19
- Bregman, J. N. 2004, *Ap&SS*, 289, 181
- Brown, T. et al. 2002, *HST STIS Data Handbook*, version 4.0, ed.. Mobasher, Baltimore, STScI
- Charlton, J. C., & Churchill, C. W. 1998, *ApJ*, 499, 181
- Charlton, J. C., Ding, J., Zonak, S. G., Churchill, C. W., Bond, N. A., & Rigby, J. R. 2003, *ApJ*, 589, 311
- Chen, H. W., & Prochaska, J. X. 2000, *ApJ*, 543, L9
- Churchill, C. W., Mellon, R. R., Charlton, J. C., Jannuzi, B. T., Kirhakos, S., Steidel, C. C., & Schneider, D. 2000a, *ApJS*, 130, 91
- Churchill, C. W., Mellon, R. R., Charlton, J. C., Jannuzi, B. T., Kirhakos, S., Steidel, C. C., & Schneider, D. 2000b, *ApJ*, 543, 577
- Churchill, C. W., Mellon, R. R., Charlton, J. C., Jannuzi, B. T., Kirhakos, S., Steidel, C. C., & Schneider, D. 1999a, *ApJ*, 519, L43
- Churchill, C. W., Rigby, J. R., Charlton, J. C., & Vogt, S. S. 1999b, *ApJS*, 120, 51



- Churchill, C. W., Steidel, C. C., Vogt, S. S., 1996, 471, 164
- Churchill, C. W., & Vogt, S. S. 2001, AJ, 122, 679
- Churchill, C. W., Vogt, S. S., & Charlton, J. C. 2003, AJ, 125, 98
- Ding, J., Charlton, J. C., & Churchill, C. W. 2004, submitted
- Ding, J., Charlton, J. C., Zonak, S. G., & Churchill, C. W. 2003a, ApJ, 587, 551
- Ding, J., Charlton, J. C., Churchill, C. W., & Palma, C. 2003b, ApJ, 590, 746
- Elmegreen, B. G. 1997, ApJ, 477, 196
- Ferland, G. 2001, Hazy, A Brief Introduction to Cloudy 96.00
- Fox, A. J., Savage, B. D., Wakker, B. P., Richter, P., Sembach, K. R., & Tripp, T. M. 2004, ApJ, 602, 738
- Frail, D. A., Weisberg, J. M., Cordes, J. M., & Mathers, C. 1994, ApJ, 436, 144
- Ge, J., Bechtold, J., Kulkarni, V. P. 2001, ApJ, 547, L1
- Gehrz, R. D., Truran, J. W., Williams, R. E. & Starrfield, S. 1998, PASP, 110, 3
- Haardt, F., & Madau, P. 1996, ApJ, 461, 20
- Haardt, F. & Madau, P. 2001, in Clusters of galaxies and the high redshift universe observed in X-rays, ed D.M. Neumann & J.T.T. Van (Savoie, France), 64
- Heiles, C. 1997, ApJ, 481, 193
- Jannuzi, B. T., et al. 1998, ApJS, 118, 1
- Kacprzak, G., Churchill, C. W., et al. 2004, in preparation
- Koratkar, A., et al. 1998, ApJ, 503, 599
- Lane, W. M., Briggs, F. H., Smette, A. 2000, ApJ, 532, L146
- Ledoux, C., Petitjean, P. & Srianand, R. 2003, MNRAS, 346, 209
- Ledoux, C., Srianand, R. & Petitjean, P. 2002, A&A, 392, 781
- Martin, C. L. 2003, in The IGM/Galaxy Connection: The Distribution of Baryons at  $z = 0$ , eds. J. L. Rosenburg and M. E. Putman (Kluwer:Dordrecht), 205

- Mateo, M. 1998, *ARA&A*, 36, 435
- Meyer, D. M., & Blades, J. C. 1996, *ApJ*, 464, L179
- Meyer, D. M., & Lauroesch, J. P. 1999, *ApJ*, 520, L103
- Pettini, M. 2003, in “Cosmochemistry: The Melting Pot of Elements”, (Cambridge University Press: Cambridge)
- Rao, S. M., & Turnshek, D. A. 2000, *ApJS*, 130, 1
- Rigby, J. R., Charlton, J. C. & Churchill, C. W. 2002, *ApJ*, 565, 743
- Rosenberg, J. L., Ganguly, R., Giroux, M. L., & Stocke, J. T. 2004, *ApJ*, in press
- Savage, B. D. & Mathis, J. S. 1979, *ARA&A*, 17, 73
- Savage, B. D., Wakker, B. P., Jannuzi, B. T., et al. 2000, *ApJS*, 129, 563
- Sembach, K. R., Savage, B. D., Lu, L., & Murphy, E. M. 1995, *ApJ*, 451, 616
- Sembach, K. R., Savage, B. D., Lu, L., & Murphy, E. M. 1999, *ApJ*, 515, 108
- Steidel, C. C. 1995, in *QSO Absorption Lines*, ed. G. Meylan (New York:Springer), 139
- Steidel, C. C., Kollmeier, J. A., Shapley, A. E., Churchill, C. W., Dickinson, M., & Pettini, M. 2002, *ApJ*, 570, 526
- Steidel, C. C., & Sargent, W. L. W. 1992, *ApJS*, 80, 1
- Tripp, T. M., Lu, L., & Savage, B. D. 1996, *ApJS*, 102, 239
- Tripp, T. M., Lu, L., & Savage, B. D. 1997, *ApJS*, 112, 1
- Vogt, S. S. et al. 1994, *Proc. SPIE*, 2198, 362
- Walker, M., & Wardle, M. 1998, *ApJ*, 481, 191
- Watson, J. K., & Meyer, D. M. 1996, *ApJ*, 473, L127
- Zonak, S. G., Charlton, J. C., Ding, J., & Churchill, C. W., 2004, 606, 196

PG0117  $z=1.3430$

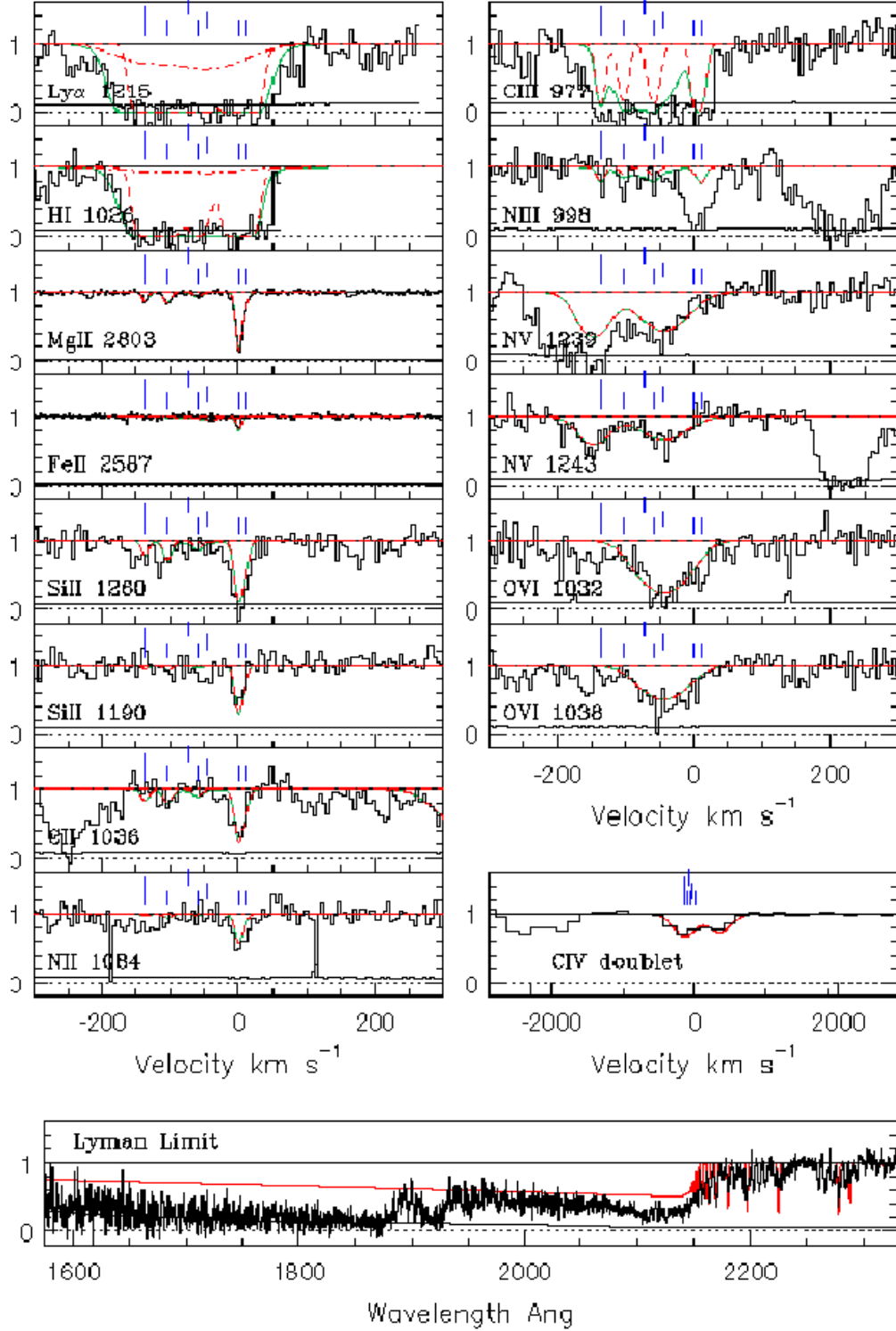


Fig. 1.— The transitions observed for the  $z = 1.3430$  system are presented here in velocity space, centered around the MgII optical depth center, as determined in Churchill & Vogt (2001). All transitions were observed with *HST*/STIS, except CIV, which was covered in a Palomar 200 inch spectrum (Steidel & Sargent 1992). The bottom row of ticks mark positions of model clouds MgII<sub>1</sub>–MgII<sub>5</sub>, the middle row represents clouds OVI<sub>1</sub> and CIV<sub>1</sub>, and the top row marks cloud Ly $\alpha$ <sub>1</sub> from Table 6. The histogram shows the data, with the black line near zero showing the  $1\sigma$  error. The smooth curve indicates the full model as described in § 4.1.1. Ionization phase contributions are shown (where applicable) with the dotted line (very-low), the dashed line (low), and the dot-dashed line (high). The lower panel presents the region of the *HST*/FOS spectrum covering the partial Lyman limit break (at  $\sim 2150$  Å, with the model contribution from this system only superimposed (the  $z = 1.3250$  system also contributes to the break)).

PG0117  $z=1.3250$

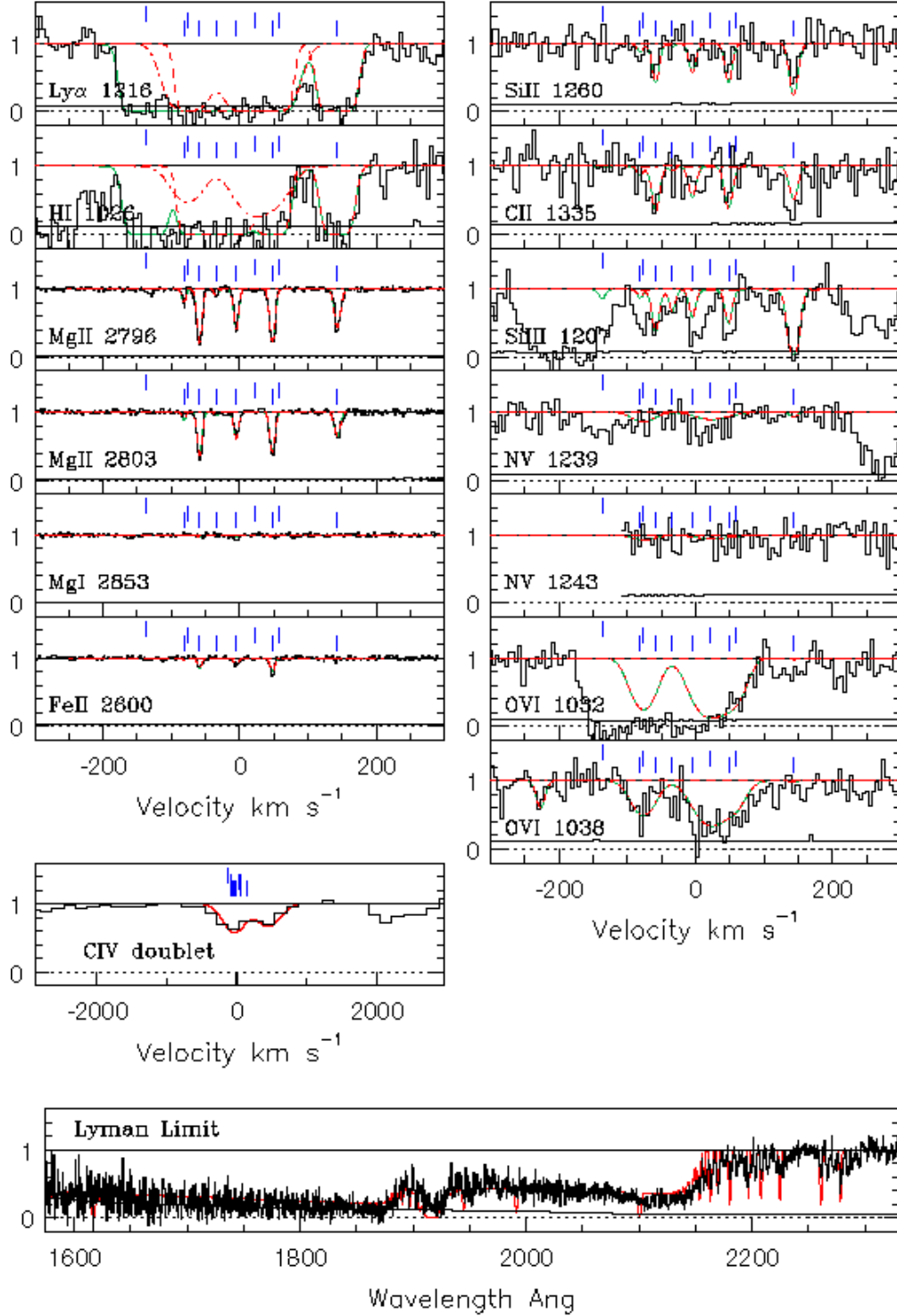


Fig. 2.— The same as Fig 1, except for the  $z = 1.3250$  system. The lower row of ticks marks the low ionization phase clouds, MgII<sub>1</sub>–MgII<sub>5</sub>, the middle row represents the high ionization phase, OVI<sub>1</sub>–OVI<sub>3</sub>, and the top row marks the additional cloud, Ly $\alpha$ <sub>1</sub> (see Table 7). The lower panel is again the *HST*/FOS spectrum, but now the combined model contributions of both this system and the  $z = 1.3430$  system are superimposed.

PG0117  $z=1.0480$

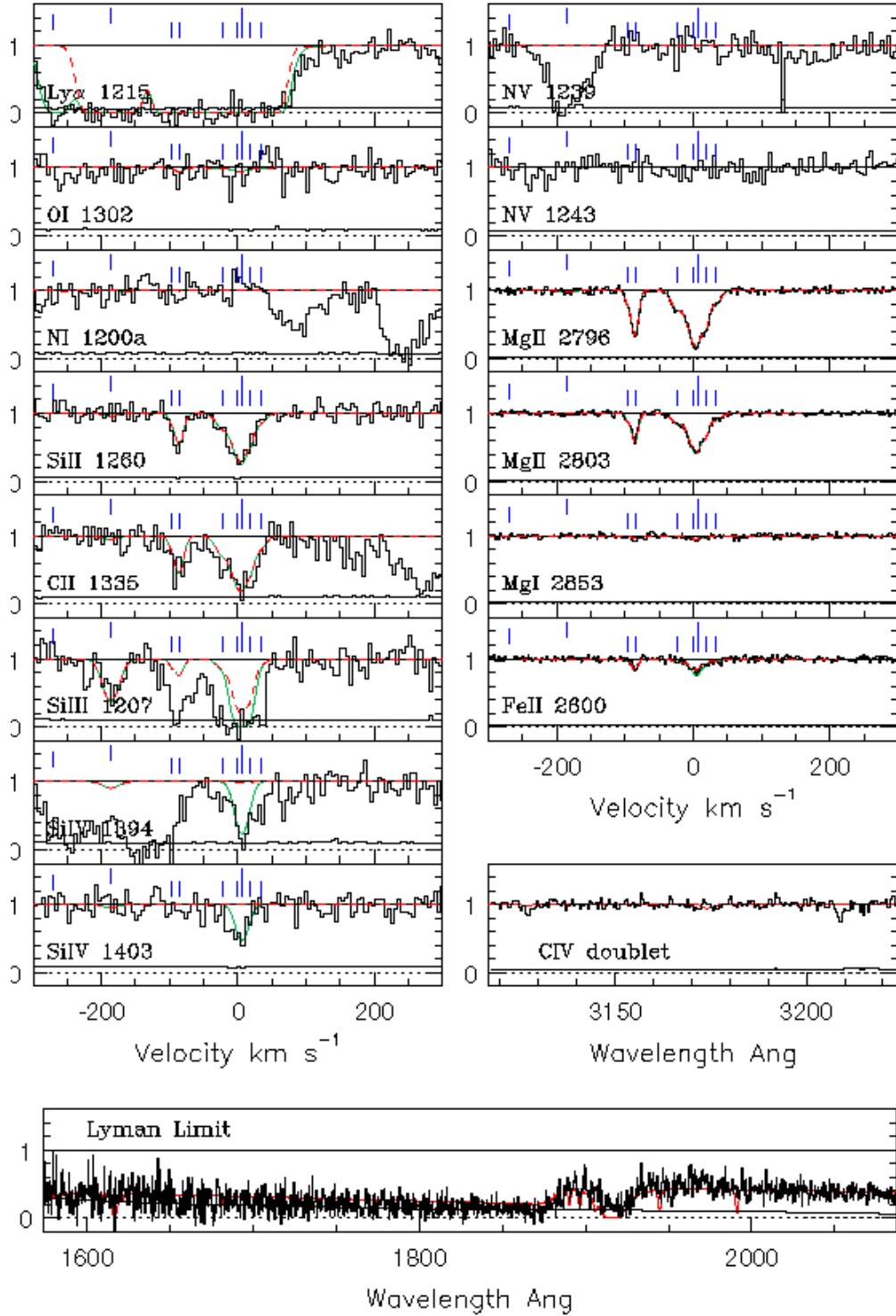


Fig. 3.— The same as Fig 1, except for the  $z = 1.0480$  system. The CIV was again covered in a ground based spectrum, but in this case was not detected. The lower row of ticks marks clouds MgII<sub>1</sub>–MgII<sub>7</sub>, the middle row marks the one cloud Ly $\alpha$ <sub>1</sub>, and the upper row marks the two clouds SiIV<sub>1</sub> and SiIII<sub>1</sub> (see Table 8). The Lyman limit break at  $\sim 1875 \text{ \AA}$  is shown in the bottom panel, in the *HST*/FOS spectrum, with model contributions from the two higher redshift systems also included.

PG0117  $z=0.7290$

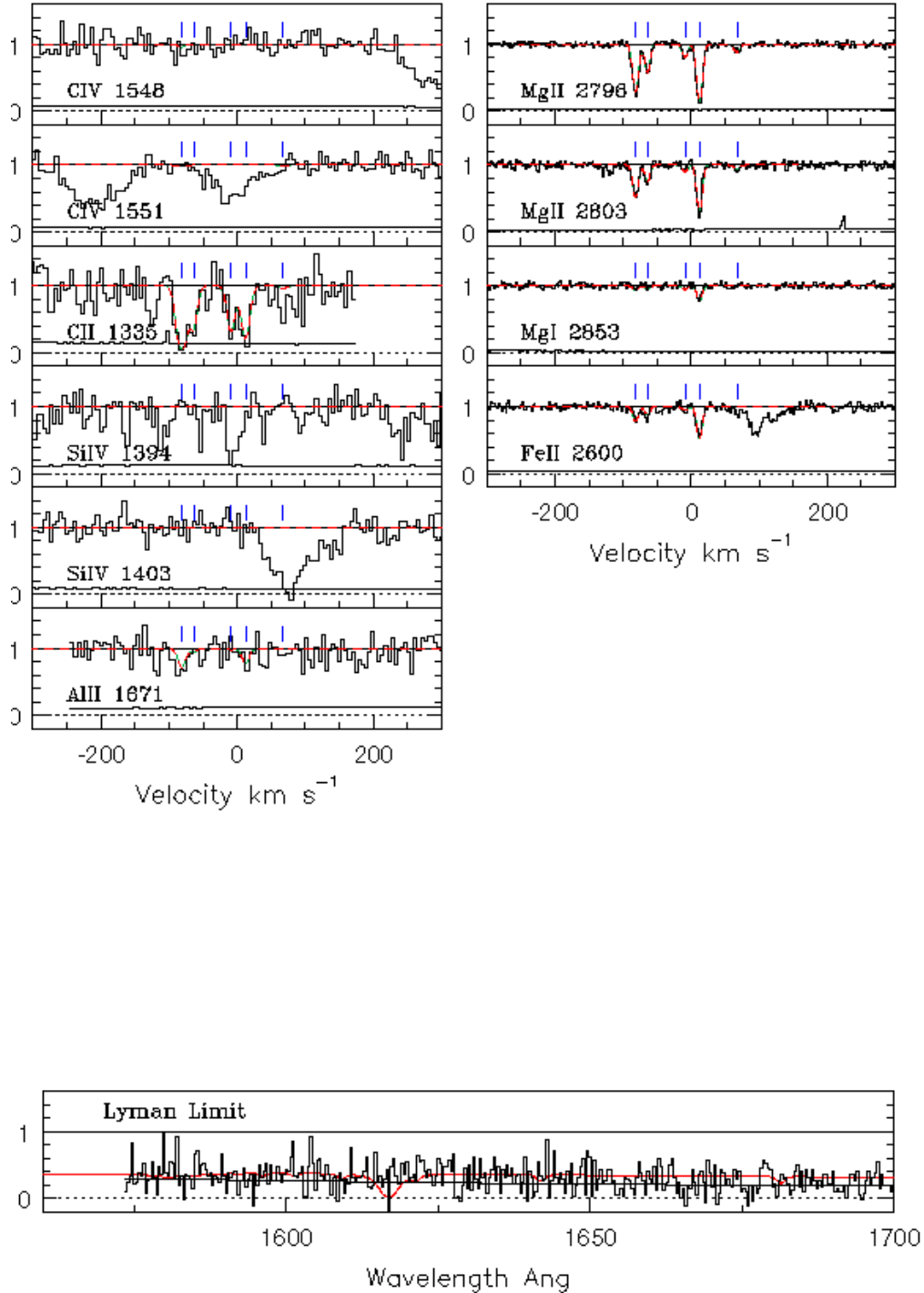


Fig. 4.— The same as Fig 1, except for the  $z = 0.7290$  system. MgII, MgI, and FeII are covered by the Keck I/HIRES spectrum, while other transitions are covered by *HST*/STIS. Here, the ticks mark the five low ionization clouds, MgII<sub>1</sub>–MgII<sub>5</sub> in our model (see Table 9). The lower panel shows the *HST*/FOS spectrum in which the Lyman limit break for this system would be at  $\sim 1576$  Å, and is apparently not present at the blue edge of this spectrum.

PG0117  $z=0.5764$

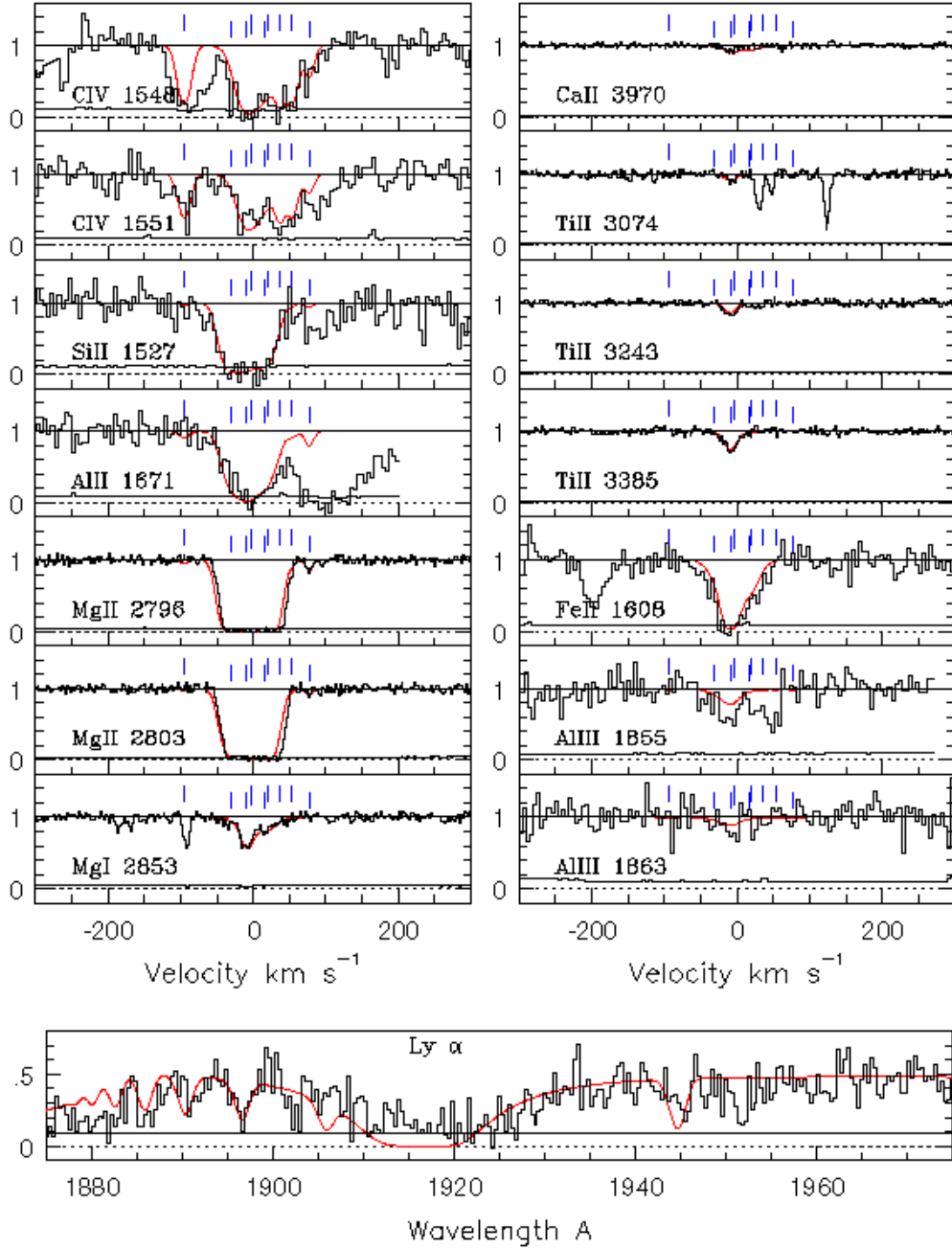


Fig. 5.— The same as Fig 1, except for the  $z = 0.5764$  system. The lower row of ticks marks positions of the very-low and low ionization clouds,  $\text{MgI}_1\text{--MgI}_3$ ,  $\text{SiII}_1\text{--SiII}_3$ , and  $\text{MgII}_1$ , which are superimposed on each other. The upper row of ticks marks the high ionization clouds,  $\text{CIV}_1\text{--CIV}_5$ . The parameters of these clouds are given in Table 10. The bottom panel shows coverage of  $\text{Ly}\alpha$  for this system in a low resolution *HST*/FOS spectrum, which was obtained in spectropolarimetry mode.

Table 1. Rest Frame Equivalent Widths for  $z = 1.3430$

Transition	EW (Å)	$\sigma_{EW}$
Ly $\alpha$	1.14	0.01
H I 1206	0.76	0.01
Si II 1206	0.144	0.008
Si II 1190	0.033	0.003
C II 1036	0.058	0.004
N II 1084	0.050	0.004
C II 977	0.69	0.01
N III 998	0.164	0.009
N V 1239	0.75	0.02
N V 1243	0.23	0.01
O VI 1032	0.37	0.01
O VI 1038	0.27	0.01
Mg II 2803	0.147	0.004
Fe II 2587	0.013	0.001
C IV $\lambda\lambda 1548, 1551$	0.67	0.02

Note. — This table shows the equivalent widths for the transitions shown in Fig 1. Included are the  $\sigma$  values for each measurement, or  $3\sigma$  limits for non-detections. Blends with other absorption features that prohibit equivalent width measurements are marked appropriately.



Table 2. Rest Frame Equivalent Widths for  $z = 1.3250$

Transition	EW (Å)	$\sigma_{EW}$
Ly $\alpha$	1.41	0.01
H I 1206	1.67	0.02
Si II 1260	0.08	0.02
C II 1335	0.065	0.008
Si III 1207	blend	n/a
N V 1239	0.078	0.007
N V 1243	< 0.012	...
O VI 1032	0.82	0.01
O VI 1038	0.34	0.01
Mg II 2796	0.312	0.007
Mg II 2803	0.191	0.007
Mg I 2853	0.006	0.002
Fe II 2600	0.035	0.003
C IV $\lambda\lambda 1548, 1551$	0.89	0.03

Note. — Same as Table 1, except for the transitions shown in Fig 2.

Table 3. Rest Frame Equivalent Widths for  $z = 1.0480$

Transition	EW ( $\text{\AA}$ )	$\sigma_{EW}$
Ly $\alpha$	1.58	0.01
O I 1302	< 0.010	...
N I 1200 $a$	< 0.008	...
Si II 1260	0.128	0.005
C II 1335	0.28	0.01
Si III 1207	0.47	0.01
Si IV 1394	0.19	0.01
Si IV 1403	0.085	0.007
N V 1239	< 0.009	...
N V 1243	< 0.007	...
Mg II 2796	0.417	0.005
Mg II 2803	0.257	0.005
Mg I 2853	0.026	0.004
Fe II 2600	0.073	0.004
C IV $\lambda\lambda 1548, 1551$	< 0.08	...

Note. — Same as Table 1, except for the transitions shown in Fig 3.

Table 4. Rest Frame Equivalent Widths for  $z = 0.7290$

Transition	EW ( $\text{\AA}$ )	$\sigma_{EW}$
CIV 1548	< 0.010	...
CIV 1551	blend	n/a
CII 1335	0.22	0.02
SIV 1394	blend	n/a
SIV 1403	< 0.010	...
AlII 1671	0.043	0.007
MgII 2796	0.240	0.008
MgII 2803	0.137	0.005
MgI 2853	0.015	0.001
FeII 2600	0.058	0.005

Note. — Same as Table 1, except for the transitions shown in Fig 4.

Table 5. Rest Frame Equivalent Widths for  $z = 0.5764$

Transition	EW ( $\text{\AA}$ )	$\sigma_{EW}$
Ly $\alpha$	11.2	1.1
CIV 1548	0.76	0.02
CIV 1551	0.52	0.02
SiII 1527	0.55	0.02
AlII 1671	blend	n/a
FeII 1608	0.34	0.01
AlIII 1855	0.22	0.01
AlIII 1863	< 0.03	...
MgII 2796	0.902	0.002
MgII 2803	0.841	0.006
MgI 2853	0.149	0.006
CaII 3970	0.018	0.003
TiII 3074	0.012	0.002
TiII 3243	0.055	0.004
TiII 3385	0.073	0.003

Note. — Same as Table 1, except for the transitions shown in Fig 5. Measurement of Ly $\alpha$  is from a low resolution *HST*/FOS spectrum.

Table 6. Model Parameters for  $z = 1.3430$

Cloud	v km s <sup>-1</sup>	$\log \frac{Z}{Z_{\odot}}$	log U	T K	Size pc	$n_H$ cm <sup>-3</sup>	log $N_{Tot}(H)$	log N(HI)	log N(MgII)	log N(CIV)	log N(NV)	log N(OVI)	$b_{HI}$ km s <sup>-1</sup>	$b_{opt}$ km s <sup>-1</sup>
MgII <sub>1</sub>	-137	-0.3	-2.8	9000	11	0.009	17.5	15.1	11.8	12.1	10.3	9.2	12.7	4.1
MgII <sub>2</sub>	-104	-0.3	-3.3	9000	2.1	0.028	17.2	15.4	12.0	11.0	9.2	0.0	13.5	6.4
MgII <sub>3</sub>	-59	-0.3	-2.8	9000	6.8	0.009	17.3	14.9	11.6	11.9	10.1	9.0	14.2	7.6
MgII <sub>4</sub>	1	-0.3	-4.0	8000	1.7	0.14	17.8	16.6	13.0	10.1	7.7	0.0	11.5	4.0
MgII <sub>5</sub>	11	-0.3	-2.8	9000	11	0.009	17.5	15.1	11.8	12.1	10.3	9.2	12.6	3.8
OVI <sub>1</sub>	-44	-0.2	...	210000	1.0	...	19.2	13.6	9.4	13.5	14.1	14.5	72.9	45.0
CIV <sub>1</sub>	-147	1.0	...	130000	0.44	...	18.4	13.3	10.7	15.0	14.0	11.7	53.7	30.0
Ly $\alpha$ <sub>1</sub>	-73	-2.5	-2.2	24000	20000	0.002	20.1	16.8	11.3	13.1	11.5	11.0	45.0	...

Note. — Model parameters for the system at  $z = 1.3430$ . Results of this model are displayed superimposed on the data in Fig 1. A “...” entry in the ionization parameter and  $n_H$  columns indicates a collisionally ionized cloud. All column densities are expressed in units of cm<sup>-2</sup>,  $b_{opt}$  is the Doppler parameter for the transition that was “optimized on” in modeling, the same transition as listed in the cloud designation column. The ionization fraction,  $f$ , can be determined from  $\log f = \log N(HI) - \log N_{Tot}(H)$ .

Table 7. Model Parameters for  $z = 1.3250$

Cloud	$v$ km s <sup>-1</sup>	$\log \frac{Z}{Z_{\odot}}$	$\log U$	T K	Size pc	$n_H$ cm <sup>-3</sup>	$\log N_{Tot}(H)$	$\log N(HI)$	$\log N(MgII)$	$\log N(MgI)$	$\log N(CIV)$	$\log N(OVI)$	$b_{HI}$ km s <sup>-1</sup>	$b_{opt}$ km s <sup>-1</sup>
MgII <sub>1</sub>	-82	-0.3	-3.5	9000	0.40	0.043	16.7	15.0	11.6	9.4	10.1	0.0	6.4	1.3
MgII <sub>2</sub>	-60	-0.3	-3.3	9000	10	0.027	17.9	16.0	12.7	10.3	11.7	0.0	12.1	2.8
MgII <sub>3</sub>	-35	-0.3	-2.4	10000	19	0.0034	17.3	14.5	11.2	8.3	12.5	10.1	6.9	1.4
MgII <sub>4</sub>	-5	-0.3	-3.5	9000	2.0	0.043	17.4	15.7	12.3	10.1	10.8	0.0	12.1	2.8
MgII <sub>5</sub>	48	-0.3	-3.6	9000	2.7	0.054	17.6	16.0	12.6	8.9	10.8	0.0	12.1	3.3
MgII <sub>6</sub>	143	-0.3	-2.2	11000	640	0.002	18.6	15.6	12.3	9.2	14.0	12.0	13.6	4.6
OVI <sub>1</sub>	-77	-0.3	-1.0	20000	9500	0.0001	18.6	14.2	9.4	5.4	14.2	14.2	28.2	22.0
OVI <sub>2</sub>	21	-0.3	-1.0	20000	19000	0.0001	18.9	14.5	9.7	5.8	14.5	14.5	34.7	30.0
OVI <sub>3</sub>	58	-0.3	-1.0	20000	4800	0.0001	18.3	13.9	9.1	5.1	13.9	13.9	26.7	20.0
Ly $\alpha_1$	-137	-3.5	-2.0	27000	23000	0.001	20.0	16.4	9.8	6.3	12.1	10.3	15.0	...

Note. — Model parameters for the system at  $z = 1.3250$ . Results of this model are displayed superimposed on the data in Fig 2. All column densities are expressed in units of cm<sup>-2</sup>.  $b_{opt}$  is the Doppler parameter for the transition that was “optimized on” in modeling, the same transition as listed in the cloud designation column. The ionization fraction,  $f$ , can be determined from  $\log f = \log N(HI) - \log N_{Tot}(H)$ .

Table 8. Model Parameters for  $z = 1.0480$

Cloud	$v$ km s <sup>-1</sup>	$\log \frac{Z}{Z_{\odot}}$	$\log U$	T K	Size pc	$n_H$ cm <sup>-3</sup>	$\log$ $N_{Tot}(H)$	$\log$ N(HI)	$\log$ N(MgII)	$\log$ N(MgI)	$\log$ N(SiIII)	$\log$ N(SiIV)	$\log$ N(CIV)	$b_{HI}$ km s <sup>-1</sup>	$b_{opt}$ km s <sup>-1</sup>
MgII <sub>1</sub>	-97	-0.7	-3.8	11000	0.47	0.061	17.0	15.5	11.6	9.6	11.4	9.4	9.2	13.4	3.0
MgII <sub>2</sub>	-86	-0.7	-4.1	10000	1.4	0.12	17.7	16.5	12.5	10.5	11.9	9.6	9.3	13.7	5.3
MgII <sub>3</sub>	-23	-0.7	-4.0	10000	1.1	0.097	17.5	16.2	12.2	10.2	11.8	9.5	9.3	16.7	10.9
MgII <sub>4</sub>	0	-0.7	-3.7	11000	9.9	0.049	18.2	16.6	12.8	10.7	12.7	10.8	10.7	16.6	10.3
MgII <sub>5</sub>	6	-0.7	-3.7	11000	3.0	0.049	17.6	16.0	12.2	10.2	12.1	10.2	10.2	13.8	4.4
MgII <sub>6</sub>	17	-0.7	-3.6	11000	6.3	0.039	17.9	16.2	12.4	10.3	12.4	10.6	10.6	14.7	6.4
MgII <sub>7</sub>	34	-0.7	-4.0	11000	0.56	0.097	17.2	15.9	11.9	10.0	11.5	9.3	9.1	15.7	9.1
SiIV <sub>1</sub>	6	-1.4	...	55000	200	...	19.6	15.8	10.3	0.0	13.6	13.3	12.3	31.5	11.0
SiIII <sub>1</sub>	-186	-1.4	-2.1	22000	2000	0.001	18.9	15.5	11.1	8.1	12.7	12.2	13.1	23.3	14.0
Ly $\alpha$ <sub>1</sub>	-266	-1.4	-3.0	15000	1.3	0.010	16.6	14.2	9.8	7.5	10.6	9.4	9.8	18.0	...

Note. — Model parameters for the system at  $z = 1.0480$ . Results of this model are displayed superimposed on the data in Fig 3. A “...” entry in the ionization parameter and  $n_H$  columns indicates a collisionally ionized cloud. All column densities are expressed in units of cm<sup>-2</sup>.  $b_{opt}$  is the Doppler parameter for the transition that was “optimized on” in modeling, the same transition as listed in the cloud designation column. The ionization fraction,  $f$ , can be determined from  $\log f = \log N(HI) - \log N_{Tot}(H)$ .

Table 9. Model Parameters for  $z = 0.7290$

Cloud	$v$ km s <sup>-1</sup>	$\log \frac{Z}{Z_{\odot}}$	$\log U$	T K	Size pc	$n_H$ cm <sup>-3</sup>	$\log N_{Tot}(H)$	$\log N(HI)$	$\log N(MgII)$	$\log N(MgI)$	$\log N(SiIV)$	$\log N(CIV)$	$b_{HI}$ km s <sup>-1</sup>	$b_{opt}$ km s <sup>-1</sup>
MgII <sub>1</sub>	-82	0.7	-3.0	50	0.97	0.0059	16.3	15.4	12.5	10.0	9.8	11.9	4.2	4.1
MgII <sub>2</sub>	-64	0.7	-4.1	300	0.029	0.075	15.8	15.4	12.1	10.5	8.4	8.7	4.1	3.5
MgII <sub>3</sub>	-9	0.7	-4.4	70	0.006	0.15	15.4	15.2	11.7	10.6	7.5	8.1	4.2	4.1
MgII <sub>4</sub>	12	0.7	-4.3	300	0.087	0.12	16.5	16.1	12.8	11.3	8.8	9.0	4.2	3.6
MgII <sub>5</sub>	67	0.7	-2.5	600	0.82	0.0019	15.7	13.7	11.5	8.3	10.8	11.1	5.8	4.9

Note. — Model parameters for the system at  $z = 0.7290$ . Results of this model are displayed superimposed on the data in Fig 4. All column densities are expressed in units of cm<sup>-2</sup>.  $b_{opt}$  is the Doppler parameter for the transition that was “optimized on” in modeling, the same transition as listed in the cloud designation column. The ionization fraction,  $f$ , can be determined from  $\log f = \log N(HI) - \log N_{Tot}(H)$ .



Table 10. Model Parameters for  $z = 0.5764$

Cloud	v km s <sup>-1</sup>	log $\frac{Z}{Z_{\odot}}$	log U	T K	Size pc	n <sub>H</sub> cm <sup>-3</sup>	log N <sub>Tot</sub> (H)	log N(HI)	log N(MgII)	log N(MgI)	log N(SiII)	log N(CIV)	b <sub>HI</sub> km s <sup>-1</sup>	b <sub>opt</sub> km s <sup>-1</sup>
MgI <sub>1</sub>	-31	-1.9	-8.2	7000	0.00079	700	18.2	18.2	11.9	10.6	11.9	0.0	7.2	1.8
MgI <sub>2</sub>	-9	-1.9	-7.6	1000	0.031	180	19.2	19.2	12.9	11.9	12.9	0.9	11.2	11.1
MgI <sub>3</sub>	16	-1.9	-7.7	6000	0.018	220	19.1	19.1	12.8	11.7	12.8	0.0	20.9	20.7
SiII <sub>1</sub>	-31	-1.9	-3.0	16000	14000	0.004	20.3	19.8	13.5	10.1	14.0	12.4	20.6	14.8
SiII <sub>2</sub>	-9	-1.9	-2.5	20000	120000	0.001	20.8	19.9	13.6	9.9	13.8	13.6	21.1	14.0
SiII <sub>3</sub>	16	-1.9	-5.0	10000	100	0.44	20.1	18.5	13.8	10.8	13.8	0.0	17.7	15.0
MgII <sub>1</sub>	77	-1.9	-2.3	22000	22000	0.001	19.7	16.4	11.6	8.5	12.0	13.0	19.3	5.0
CIV <sub>1</sub>	-95	-1.9	-1.8	30000	140000	0.0003	20.1	16.2	11.2	7.6	11.8	13.7	23.0	9.0
CIV <sub>2</sub>	-3	-1.9	-1.8	30000	270000	0.0003	20.4	16.6	11.6	7.8	12.2	14.0	27.9	18.8
CIV <sub>3</sub>	20	-1.9	-1.8	30000	49000	0.0003	19.6	15.8	10.7	7.3	11.3	13.3	23.4	10.0
CIV <sub>4</sub>	37	-1.9	-1.8	30000	120000	0.0003	20.0	16.2	11.2	7.5	11.8	13.7	20.7	6.0
CIV <sub>5</sub>	54	-1.9	-1.8	30000	120000	0.0003	20.0	16.2	11.2	7.5	11.8	13.7	22.7	8.0

Note. — Model parameters for the system at  $z = 0.5764$ . Results of this model are displayed superimposed on the data in Fig 5. A “...” entry in the ionization parameter column indicates a collisionally ionized cloud. All column densities are expressed in units of cm<sup>-2</sup>.  $b_{opt}$  is the Doppler parameter for the transition that was “optimized on” in modeling, the same transition as listed in the cloud designation column. The ionization fraction,  $f$ , can be determined from  $\log f = \log N(\text{HI}) - \log N_{Tot}(\text{H})$ .